



**HAL**  
open science

## 2.2 Contact Mechanics

Leda Lacaria, Alessandro Podestà, Manfred Radmacher, Felix Rico

► **To cite this version:**

Leda Lacaria, Alessandro Podestà, Manfred Radmacher, Felix Rico. 2.2 Contact Mechanics. Biomedical Methods, De Gruyter, pp.21-64, 2023, 10.1515/9783110640632-003 . hal-04761046

**HAL Id: hal-04761046**

**<https://hal.science/hal-04761046v1>**

Submitted on 30 Oct 2024

**HAL** is a multi-disciplinary open access archive for the deposit and dissemination of scientific research documents, whether they are published or not. The documents may come from teaching and research institutions in France or abroad, or from public or private research centers.

L'archive ouverte pluridisciplinaire **HAL**, est destinée au dépôt et à la diffusion de documents scientifiques de niveau recherche, publiés ou non, émanant des établissements d'enseignement et de recherche français ou étrangers, des laboratoires publics ou privés.

# 1 Contact Mechanics

*Leda Lacaria<sup>1</sup>, Alessandro Podestà<sup>2</sup>, Manfred Radmacher<sup>3</sup>, Felix Rico<sup>1</sup>*

<sup>1</sup> Aix-Marseille Univ, INSERM, CNRS, LAI, Turing centre for living systems, 163 avenue de Luminy, 13009 Marseille, France

<sup>2</sup> Dipartimento di Fisica “Aldo Pontremoli” and C.I.Ma.I.Na, Università degli Studi di Milano, via Celoria 16, 20133 Milano, Italy.

<sup>3</sup> Institute of Biophysics, University of Bremen, 28359 Bremen, Germany.

The study of the deformation between two bodies in contact upon application of force can reveal relevant information about the mechanical properties of the two objects and their composition. This problem, first considered by Heinrich Hertz for two contacting sphere (Hertz, 1882) and (Hertz, 1881), is at the base of mechanical tests employing suitable indenters, including those being performed by atomic force microscopy (AFM) and commercial nanoindenters. To simplify the problem, one of the bodies can be considered as a rigid nondeformable probe and the other as an infinite half space, the sample, of which we want to study the elastic properties. The underlying formalism to determine the pressure upon a given deformation was generalized by Boussinesq, from which it takes its name: the Boussinesq’s problem (Boussinesq, 1885; Love, 1929). The scientific field that studies the properties of materials through the force-deformation interaction between two bodies in contact, is commonly called Contact Mechanics (Johnson, 1985).

In the simple configuration, relevant to mechanical measurements exploiting AFM or nanoindenters, the approaching probe will apply a pressure on the sample and, due to the repulsion of atoms, which is basically a consequence of the Pauli exclusion principle, will cause its deformation. The ratio between the applied force and the deformation, or the applied stress and the resulting strain, is a quantitative description of the mechanical properties of the sample. Traditionally, theoretical models from contact mechanics are used to fit experimental data and obtain the mechanical properties of materials at macroscopic or mesoscopic scales.

Nowadays, the development of advanced techniques to manipulate rigid probes of nanoscale dimensions, such as AFM, nanoindenters and optical and magnetic tweezers, opened a new door for mechanics of cells and tissues, from the macroscale to the micro and nanoscale. Indeed, while traditionally models of contact mechanics were principally used to describe the macroscopic mechanical properties of materials in mechanical engineering and material sciences, now contact mechanics has been rediscovered as a powerful tool to investigate the local, nanoscale mechanical properties of soft living materials like cells and tissues, making contact mechanics well known also in the field of biophysics and mechanobiology (Radmacher et al., 1992).

In this chapter, we will describe the most relevant contact models to analyse AFM force-deformation measurements to determine the mechanics of soft matter, including cells and tissues. We will illustrate different contact elastic and viscoelastic models, specifying the most common tip geometries and sample configurations. We will provide a brief introduction to the theoretical tools required to obtain the described models but leave the full development by referring to the original texts.

## 1.1 Elasticity and AFM force-deformation measurements

Contact mechanics involves the determination of the pressure-deformation relationship between two bodies in contact. In conventional AFM measurements, an external force ( $F$ ) is

exerted by the rigid probe in contact with the sample and a resulting deformation or indentation ( $\delta$ ) is induced due to the pressure on the sample's surface.

A typical AFM measurement, therefore, is represented by a force-distance curve, where the distance is the  $z$  position of the probe relative to the sample, as shown in Figure 1-1.

When the probe is far away from the sample the cantilever deflection, and thus the force, is zero. After the point of contact between probe and sample, the pressure of the probe starts to deform a soft sample and the force increases with the sample indentation.

The contact region starts from the point of contact between the probe and the sample and ends in the point of maximum force and maximum indentation of the sample.

The precise determination of the Contact Point allows the conversion of the force-distance curve in a force-indentation curve that can be fitted with the expressions from Contact Mechanics models  $F(\delta)$ .

A typical force-curve on a rigid material will be linear, where deflection and distance will be identical. On a soft sample, like for example a cell or a biological tissue, the slope will be smaller than 1 and often nonlinear, depending on the probe geometry as a consequence of increasing contact area between the probe and the sample surface.

Moreover, in biological samples and soft materials in general, we can have energy dissipation or viscous effects, which will result in a difference, often termed hysteresis, between the approach and the retract curve.

In soft materials adhesion between the probe and the sample is often present, which will become visible as negative forces during retract.

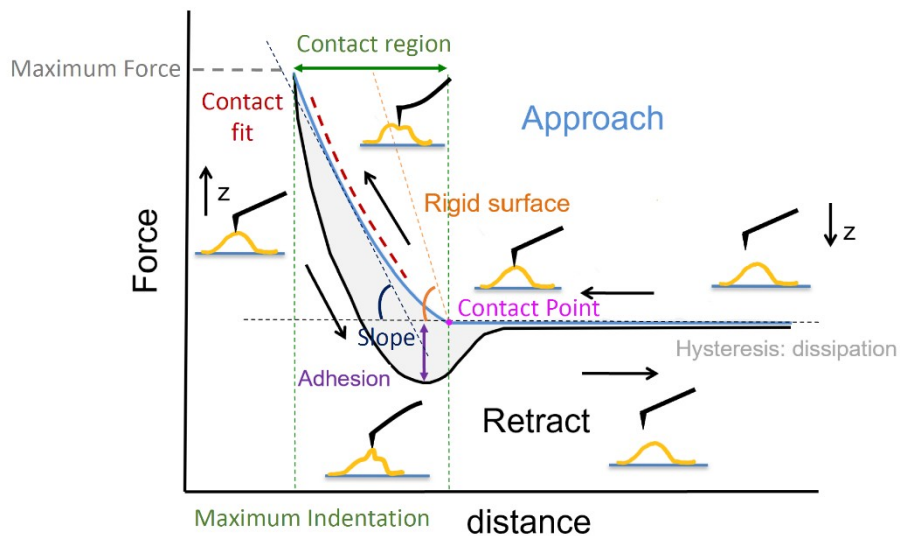


**Figure 1-1:** Schematic typical AFM measurement (Force-distance curve) on a soft material, for example a cell. In blue the Approach curve and in black the Retract. In green is shown the contact region, starting from the contact point between the probe and the soft sample and delimited by the point of maximum force and maximum indentation. The black and orange dashed lines show the typical difference in slope for a rigid surface (orange) and a soft surface (black). In violet the adhesion effect on the retract curve, in grey the hysteresis in the curve due to dissipation of energy.

Determining an analytical (or numerical) relation of the local stress and strain distribution in the contact region, is the common route to derive a relation between the experimentally accessible force-indentation, allowing to deduce the materials' properties. This interplay between theoretical derivations and experimental data is the essence of contact mechanics.

The elasticity of a material is its tendency to resist deformation when subjected to an external force combined with its ability to return to its original size and shape when the force is removed. This property of the material can be described by the Young's modulus ( $E$ ), which is related the shear modulus ( $G$ ) and the bulk modulus ( $K$ ), defined as the ratio between the

stress ( $\sigma$ ) and the strain ( $\varepsilon$ ) in uniaxial compression:  $\sigma = E\varepsilon$ , as already explained in detail in Chapter 2.1. A material is defined as elastic when its response to the application of an external force, in terms of deformation and recovery, is instantaneous and there is no energy dissipated. In the general theory of elasticity, the sample is solid and regarded as a continuous material. Therefore, when the body is not deformed, it is in thermal equilibrium. During the deformation of the body, there is a change in the shape of the boundary surface, the arrangement of the components of the solid is modified, and internal small forces are generated because the system tends to return to the state of equilibrium. These local forces are due to the repulsion of the molecules and components within the body and are termed internal stresses. The total force applied on the body is identical to the continuous sum, i.e. the integral, over-all internal stresses developed inside the body upon deformation.

## 1.2 Contact elastic models

In this section we describe some of the most common contact elastic models according to the geometry of the contact. In the context of AFM, contact models have been developed for those geometries, which correspond to commercially available probes. All models in this section assume that a nondeformable probe of known geometry indents an infinite purely elastic, isotropic, linear half space of known Young's modulus  $E$  and Poisson's ratio  $\nu$ . The Poisson's ratio is the amount of transversal elongation divided by the amount of axial compression. When studying cells and tissues, the sample is often assumed to be incompressible (which is a good approximation for most elastomers and gels, as well as for cells and tissues), which leads to  $\nu = 0.5$ .

### 1.2.1 The Hertz Model

The application of mechanics to contact problems first began with Heinrich Hertz in 1881, who, in his pioneering paper entitled "On the contact of elastic bodies", solved the problem of the elastic contact between two spheres (two lenses) (Hertz, 1881) (Hertz, 1882). This model can be extended to a sphere in contact with an infinite half space, which is a common configuration of AFM measurements.

Hertz's approach was based on the following assumptions, which define Hertzian contact:

- 1) The surfaces are frictionless and perfectly smooth.
- 2) The surfaces are continuous.
- 3) The probe and the sample are isotropic, axisymmetric and show a linear elastic response.
- 4) The strains are very small in comparison with any relevant dimension of the body
- 5) The bodies are considered as infinite half-spaces.
- 6) The surfaces do not show adhesion

The assumption 1) allows us to state that only a normal pressure acts between the parts in contact. When the assumption 2) is held, the area of contact is much smaller than the characteristic dimensions of the contacting bodies, i.e. the area of contact between the two bodies is close to zero, which implies that the pressures are finite. Indeed, even if the forces due to the repulsion of the atoms of the two bodies in contact become very large locally, the integral of these forces through an infinitely small area is always finite. According to the assumption 3), since the two surfaces are isotropic and axisymmetric, their common normal is parallel to the direction of the pressure that each body exerts on the other. Thus, the surface of

contact, and also the surface of pressure, is lying on the tangent plane  $xy$  of the two surfaces and the normal is parallel to the  $z$  direction. In this condition the distance of any point of either surface from the common tangent plane is in the neighbourhood of the point of contact and can be described by a homogeneous quadratic function of  $x$  and  $y$ . This last assumption is important, since a sphere can only be described as a paraboloid of revolution for small deformations relative to the radius of curvature. Assumption 4) allows us to apply the linear theory of elasticity. Indeed, when the strains<sup>1</sup> are smaller than the body dimensions in a continuum body, the displacement gradient is smaller than 1 and the strain tensor can be linearized accordingly to the infinitesimal strain theory (Slaughter, 2002); if the strains are instead comparable to the body dimensions, the finite strain theory or the plasticity theory should be used. Assumption 5) assures that the influence of the boundaries of the two bodies can be ignored. Finally, assumption 6) states that the contact is adhesionless, which allows to exclude other forces than the elastic ones are present inside or outside the contact area.

The analysis presented further is based on the approach used by Dimitriadis and Chadwick following Landau and Lifshitz (Dimitriadis et al., 2002; Landau and Lifshitz, 1986), as it will become useful later on. In analogy to AFM measurements, a spherical probe of radius  $R$  is assumed to apply a total force  $F$  in the  $z$  direction to a half-space, making contact at  $z = 0$ , as

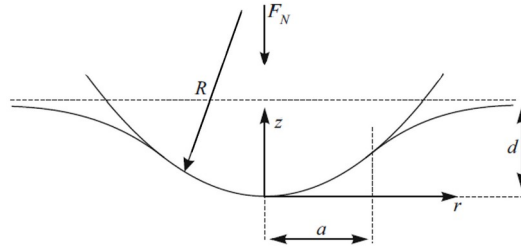


**Figure 1-2** Schematic parabolic probe indenting an elastic infinite half space.

shown in Figure 1-2. The force is distributed over the contact circle of radius  $a$  centred at  $r = 0$  (Figure 1-2), where  $r$  is the in-plane radial distance in the  $z$  plane. The axial deformation field  $u_z$  can be obtained by integrating the product of the displacement profile for a point concentrated force, i.e. the Green's function  $G$ , and the pressure distribution  $P_z$  over the contact area  $A$ :

$$u_z(r, z) = \iint_A P_z(r_s) G(s) dA, \quad (1.1)$$

where the Green's function is given by:

$$G(s) = \frac{-1+\nu}{2\pi E s} \left( \frac{z^2}{s^2} + 2(1-\nu) \right) \quad (1.2)$$

The distribution of pressure applied by the sphere was obtained by Hertz as

$$P_z(r_s) = p_0 \sqrt{a^2 - r_s^2} \quad (1.3)$$

<sup>1</sup> The strain in general is a tensor and it is defined as the change in an element of length when the body is deformed, that is the gradient of the displacement vector  $\nabla \mathbf{u}$ . The displacement  $\mathbf{u}$  of a point in a body due to the deformation is the distance between the coordinate of the point before and after the deformation:  $\mathbf{u} = \mathbf{x}'_i - \mathbf{x}_i$ , more details are described in (L.D. Landau and E.M. Lifshitz, 1986))

where  $s=|r|=(r^2+r_s^2-2rr_s\cos\phi+z^2)^{1/2}$  is the distance between the source  $(r_s,0,0)$  and the observation point  $(r,\phi,z)$ ; being  $\phi$  the azimuthal angle of the cylindrical coordinates, and  $p_0=\frac{2E}{\pi R}\frac{1}{(1-\nu^2)}$ .

If the deformation field in Eq. 1.1 is assumed to conform with a paraboloid of revolution

$$u_z=\delta-\frac{1}{2R}r^2 \quad (1.4)$$

the contact radius depends only on the indentation of the sample ( $\delta$ ) and on the radius of curvature of the probe and can be written in terms of the applied force and the mechanical parameters of the half-space,

$$a^2=\delta R=\left(\frac{3(1-\nu^2)}{4E}FR\right)^{2/3} \quad (1.5)$$

Eq. 1.5 can be rearranged in terms of the normal applied force as a function of the deformation or indentation  $F(\delta)$ .

$$F=\frac{4}{3}\frac{E}{1-\nu^2}\sqrt{R}\delta^{\frac{3}{2}} \quad (1.6)$$

Thus, according to the Hertz model, the relation between force and indentation depends only on the intrinsic properties of the material, the compressibility expressed by the Poisson's ratio  $\nu$  and the elasticity expressed by the Young's modulus  $E$ , and on the radius of curvature  $R$ .

The Hertz model can also be used, and was originally developed, to describe the contact between two elastic spheres (with respective radii  $R_1$  and  $R_2$ , Poisson's ratio  $\nu_1$  and  $\nu_2$  and Young's moduli  $E_1$  and  $E_2$ ) compressed by a force  $F$  resulting in a contact area of radius  $a$ , as shown in Figure 1-2. In that case, an effective Young's modulus  $E_{\text{eff}}$  takes into account the elastic properties of both the bodies and can be defined as:

$$\frac{1}{E_{\text{eff}}}=\frac{1-\nu_1^2}{E_1}+\frac{1-\nu_2^2}{E_2} \quad (1.7)$$

The effective radius  $R_{\text{eff}}$  is defined as:

$$\frac{1}{R_{\text{eff}}}=\frac{1}{R_1}+\frac{1}{R_2} \quad (1.8)$$

Assuming that one of the two bodies has infinite curvature radius  $R_2 \rightarrow \infty$ , the problem of the two spheres reduces to the problem of a half infinite elastic space, as shown in Figure 1-3, and the only geometrical variable becomes the radius  $R$  of the spherical probe. Moreover, if we consider the probe as infinitely rigid,  $E_1 \gg E_2$ , so  $E_1 \rightarrow \infty$ , the solution will depend only on the Poisson's ratio and the Young's modulus of the half infinite space.

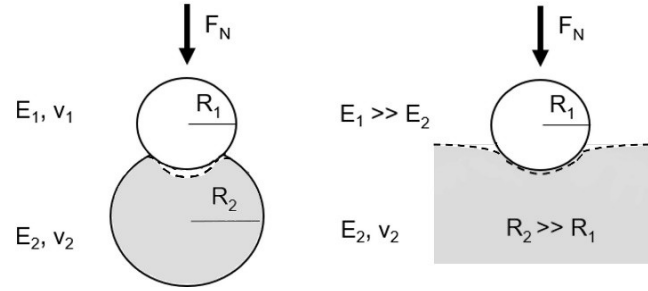


**Figure 1-3** Schematic drawing of the Hertz contact problem: the general case of two spheres in contact and the particular case of a rigid spherical probe indenting an infinite half-space.

The Hertz model is largely used to measure mechanical properties of materials, but to obtain reliable values of elasticity is important to carefully evaluate if the assumptions described above are valid. The distribution of stresses transmitted inside the deformed material depends on the area of contact between the rigid probe and the sample. Indeed, the normal force is the result of the local pressure distributed over the area of contact, which changes during the penetration of the probe inside the sample. For that reason, the expression of the function  $F(\delta)$  depends strictly on the geometry of the problem, in particular on the shape of the probe. It is important to note that the derivation of the Hertz model assumes that the indenter is a paraboloid of revolution. Thus, its application to spheres and similar geometries is limited in principle to small indentations compared to the radius of curvature.

Since the publication of the Hertz solution for the spherical probe contact problem, several models have been formulated to obtain a force-indentation relation for probes of different geometries. Boussinesq derived a solution of the problem corresponding to the case a solid of revolution indenting a half space, whose axis was normal to the original boundary of the space (Boussinesq, 1885). Thanks to the Boussinesq solution, it was possible to derivate later the model for a flat-ended cylindrical probe (Love, 1929) and a conical probe (Love, 1939). Sneddon in 1965 formulated a general solution for a probe of arbitrary profile, from which he derived, as particular cases, other geometries, including a sphere not approximated by a paraboloid of revolution (Sneddon, 1965), which presents the advantage of not being limited by the constraint  $\delta \ll R$ .

Sneddon derived the general integrals required to calculate the indentation and the applied force as a function of the shape profile function of the punch, as well as the corresponding pressure distributions for different geometries.

For most of them, he showed that the force-indentation relationship can be generally written as

$$F = C E_{eff} \delta^m \quad (1.9)$$

where  $F$  is the normal applied force,  $C$  reflects the indenter geometry constants,  $E_{eff}$  refers to the effective modulus of the body,  $\delta$  is the indentation and  $m$  is an exponent that depends on how the area of contact changes during the indentation of the probe, in turn depending on the shape profile function of the indenter. In the following, we provide a list of solutions for different geometries derived by Sneddon, together with more recent contact problem solutions for geometries closer to the actual shapes of available AFM probes used in experiments. A review of the different models is provided in Table 1.

### 1.2.2 Paraboloid of revolution

As solved by Hertz, the solution for a paraboloid of revolution of curvature  $1/2R$  is

$$F = \frac{4}{3} \frac{E}{(1-\nu^2)} \sqrt{R} \delta^{\frac{3}{2}} \quad (1.10)$$

This is the well-known Hertz model derived above (Eq. (1.6)). The contact radius is  $a = \sqrt{R\delta}$ , and the force-contact radius relation is

$$F = \frac{4}{3} \frac{E}{(1-\nu^2)} \frac{a^3}{R} \quad (1.11)$$

### 1.2.3 Flat ended cylinder

The expression for a flat ended cylinder of radius  $a$  is

$$F = 2a \frac{E}{1-\nu^2} \delta \quad (1.12)$$

Notice that, unlike the model for the paraboloid of revolution (Eq. 1.14), the relationship is linear, as the area of contact does not change with indentation (the contact radius  $a$  is constant). Cylindrical punches are thus ideal to probe the nonlinearity of the sample.

### 1.2.4 Sphere

Sneddon provided the exact solution for a spherical probe of radius  $R$  in terms of the radius of contact  $a$  (which is now different from  $\sqrt{R\delta}$ )

$$F = \frac{E_s}{2(1-\nu_s^2)} \left[ (a^2 + R^2) \ln \left( \frac{R+a}{R-a} \right) - 2Ra \right] \quad (1.13)$$

after correction for a typographical error (Heuberger et al., 1996). Where the indentation is a function of the radius of contact

$$\delta = \frac{1}{2} a \ln \left( \frac{R+a}{R-a} \right) \quad (1.14)$$

The advantage of this solution compared with the Hertz model is that it is valid for any applied indentation, provided  $a \leq R$ . The disadvantage is that it requires numerical computations (Chyasnavichyus et al., 2016) or polynomial approximations (Kontomaris and Malamou, 2021a). The polynomial corrections for the case of large indentations, typically up to  $\delta = R$  obtained by Kontomaris et al. (Kontomaris and Malamou, 2021a, 2021b) and by (Müller et al., 2019) are the following:



$$\Omega_{Kontomaris} = c_1 + \sum_{k=2}^6 \frac{3}{2k} c_k \gamma^{k-3/2} \quad (1.15)$$

With coefficients:

$$c_1 = 1.0100000 \quad c_2 = -0.0730300 \quad c_3 = -0.1357000 \quad c_4 = 0.0359800 \quad c_5 = -0.0040240 \quad c_6 = 0.0001653$$

and

$$\Omega_{Müller} = 1 - \frac{1}{10} \gamma - \frac{1}{840} \gamma^2 - \frac{1}{15120} \gamma^3 + \frac{1357}{6652800} \gamma^4 \quad (1.16)$$

where  $\gamma = \delta/R$  is the ratio between the indentation and the radius of the probe and  $\Omega(\gamma)$  is the polynomial correction factor that can be multiplied for the Hertz equation (eq. (1.6) in the case of large indentation in the following form:

$$F = F_{Hertz} \Omega(\gamma(\delta, R)) \quad (1.17)$$

Even if the formulation of the two correction factors is different (the Müller correction is a fourth-order power law expansion, while the Kontomaris correction is not, indeed the second term is of power 1/2), the two corrections are equivalent, compared with the Sneddon formula.

As expected, the spherical solution by Sneddon approximates the Hertz model for small indentations ( $\delta \ll R$ ). The general solution for an ellipsoid of revolution was also derived in the Sneddon work (see above, Section 1.2.3).

### 1.2.5 Other geometries

Sneddon provided the general exact solution for a punch with a shape profile described by a polynomial  $z = \sum c_n r^n$ . For more complex geometries, approximations are often necessary. A general development that leads to some of the solutions derived by the Sneddon approach was proposed for Barber and Billings to derive the approximate solution for a punch of arbitrary shape and they applied it to an  $n$ -sided regular pyramid with semi-included angle  $\theta$  (Barber and Billings, 1990). This powerful approach is briefly described in the following and has been recently used to derive more complex problems that will be listed later.

The pressure distribution  $P(r)$  for a probe of projected area  $A$  can be obtained knowing the expression of the work  $F\delta$  for a flat cylinder probe, using the Betti-Rayleigh reciprocal theorem (Betti, 1872; Rayleigh, 1873), which relates the two properties (Gavara and Chadwick, 2012).

Betti's reciprocal theorem states that, for a linear elastic material, for two displacement systems at points A and B due to two respective forces  $F$  and  $F^i$ , the work done by  $F$  applied in A through the relative deformation produced by  $F^i$  in A is equal to the work done by  $F^i$  applied in B through the relative deformation produced by the  $F$  in B:

$$F_A d_A^i = F_B^i d_B \quad (1.18)$$

In general, we can write the relative deformation as the integral over all strains of all elements of the total surface  $d = \int_S u_i dS$  and the total force as  $F = \int_S T_i dS$ , thus

$$\int_S T_i u_i dS = \int_S T_i^{\dot{c}} u_i^{\dot{c}} dS \quad (1.19)$$

Where  $S$  is the surface of the projected area of the indenting punch,  $T_i$  and  $T_i^{\dot{c}}$  are the normal internal stresses due to respectively the forces  $F$  and  $F^{\dot{c}}$ , while  $u_i$  and  $u_i^{\dot{c}}$  are the corresponding displacements.

In our AFM problem, the force is applied just in the  $z$  direction and the area corresponds to the projected area of a probe of arbitrary shape.

Accordingly, a probe of flat-ended cylindrical shape can be considered in the point A (left part of the eq. (1.19) and an arbitrary probe shape in the point B (right part of the eq. (1.19), of which we want to obtain the force-indentation expression.

The force  $F$  and the corresponding displacements  $u_i$  are valid only for a frictionless contact, since we consider only the component of the stress tensor normal to the surface. The surface displacements  $u_i$  can be described by the shape profile function of the probe  $f(x,y)$  or  $f(r,\phi)$ , while the stress  $T_i^{\dot{c}}$  is the pressure distribution  $P^*(r,\phi)$ . The displacement  $u_i^{\dot{c}}$  corresponding to the force  $F$  applied by a flat-ended cylindrical probe is well known and given by the eq. (1.12), and corresponds to the uniform deformation, thus to the uniform indentation  $\delta^*$  induced by  $F$ , the force applied by the probe, and since it is a constant, it can be taken outside of the integral (left-hand side of eq. 1.17). Thus, the integral of the internal stresses over the surface is by definition the total force  $F = \int_S T_i dS$ . This leads to the following form of the total force

force

$$F = \int_A P^{\dot{c}}(r, \phi) \frac{f(r, \phi)}{\delta^{\dot{c}}} r dr d\phi \quad (1.20)$$

The analytical form of  $P^*(r,)$  is only known for an elliptical contact area and is given by

$$P^{\dot{c}}(r, \phi) = \frac{E}{\pi(1-\nu^2)} \frac{\delta^{\dot{c}}}{\sqrt{a^2 - r^2}} \quad (1.21)$$

Thus, the pressure distribution can be approximated by that of a flat cylindrical punch with an area corresponding to the best ellipse approximation to the actual contact area. The radius of contact is then determined by imposing that the derivative of the force over the contact radius is maximal ( $\frac{\partial F}{\partial a} = 0$ ) (Shield, 1967). More refined approaches for the flat punch pressure distribution are available in the literature (Barber and Billings, 1990; Fabrikant, 1986).

This approach is thus a valid approximation for an indenter of arbitrary shape, provided the shape profile function is known. For example, in the case of a conical probe, the corresponding displacement under the punch is  $u = \delta - r \cot \theta$ , where  $r$  is the radial distance from the vertex. At this point the eq. (1.20) can be written as:

$$F = 2 \frac{E}{1-\nu^2} \int_0^a \frac{\delta - r \cot \theta}{\sqrt{a^2 - r^2}} r dr = 2 \frac{E}{1-\nu^2} \left( \delta a - \frac{\pi}{4} a^2 \cot \theta \right) \quad (1.22)$$

By imposing  $\frac{\partial F}{\partial a} = 0$ , we find the radius of contact  $a = \frac{2 \tan \theta}{\pi} \delta$ , and eq. (1.22) can be written as

$$F = \frac{2 \tan \theta}{\pi} \frac{E}{1-\nu^2} \delta^2 \quad (1.23)$$

In the case of a cone, the solution is exact as the best ellipse approximation for the flat punch is actually a circle of radius  $a$ .

### 1.2.6 Cone

The solution for a conical probe of semi-included angle  $\theta$ , often called the Sneddon model, as obtained in the previous section, is

$$F = \frac{2 \tan \theta}{\pi} \frac{E}{1-\nu^2} \delta^2 \quad (1.24)$$

It is important to note that here the semi-included angle  $\theta$  is defined from the vertical axis ( $z$ ) to the face of the cone and not from the plane tangent to the face, as some other works do<sup>2</sup>. In this case, the contact radius is given by  $a = \frac{2 \tan \theta}{\pi} \delta$ .

### 1.2.7 $n$ -sided regular pyramid

The approach described above has been used originally by Barbers and Billing to provide a solution for a regular  $n$ -sided pyramid of semi-included angle  $\theta$ . The general solution is:

$$F \approx \frac{2 \tan \theta}{n \sin \frac{\pi}{n}} \frac{E}{1-\nu^2} \delta^2 \quad (1.25)$$

For  $n \rightarrow \infty$ , we recover the solution for a cone. For the common 4-sided pyramidal tip often used in AFM the expression is:

$$F \approx \frac{\tan \theta}{\sqrt{2}} \frac{E}{1-\nu^2} \delta^2 \quad (1.26)$$

This result is within 6% of the numerical solution provided by Bilodeau (Bilodeau, 1992). The contact radius is given by  $a = \frac{\delta \tan \theta}{\sqrt{2}}$ .

---

<sup>2</sup> We opted for using semi-included angle, instead of semi-open, as it is more explicit the definition we use here.

### 1.2.8 Blunted cone and pyramid

While the above equations are satisfactory and provide good approximations to several tip shapes and experimental conditions, the ideal geometry of a cone or a pyramid is often not found in experimental AFM probes. In particular, for small indentations of some tens of nanometers, the ideally sharp apex appears blunted. For this reason, solutions for more realistic probe shape profiles have been proposed. We here provide the general solution for an

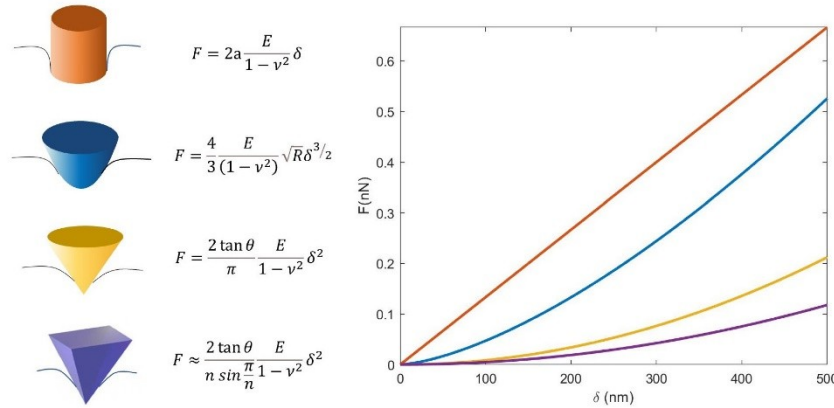
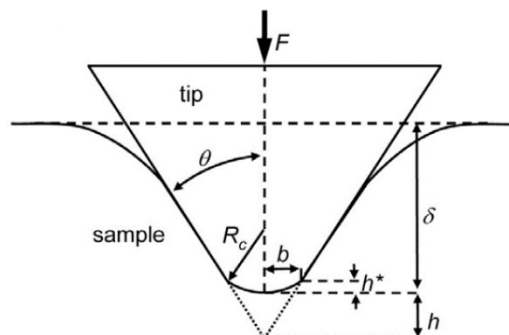


**Figure 1-4** Force-indentation relations for different probe geometries: a cylindrical indenter (Sneddon model), a paraboloidal indenter (Hertz model), a conical indenter (Sneddon model) and a pyramidal indenter (Bilodeau model). The parameters used for the figures are:  $E = 1000 \text{ Pa}$ ,  $\nu = 0.5$ ,  $R = 700 \text{ nm}$ ,  $a = 500 \text{ nm}$ ,  $\theta = 45^\circ$ .

$n$ -sided regular pyramid described above but with a blunt tip of radius  $R_c$  at the apex. The solution was found following the above described method using Betti's reciprocal theorem and the Rayleigh-Ritz approximation, which is shown in table 1 (Rico et al., 2005). As shown above for the case of a sharp indenter, for  $n \rightarrow \infty$  we recover the solution for a blunted cone, which was proposed before by Briscoe and co-workers (Briscoe et al., 1994). It is interesting to comment on the original definition of the cap width, which considered the case of a sphere that emerged tangential with the pyramid faces. The original work defined this parameter as  $b = R_c \cos \theta$ . Nevertheless, to solve the problem, the actual integration was performed for a paraboloid of radius  $R_c$ . This introduced a slight discontinuity in the numerical solutions for the contact radius. To avoid this discontinuity, the cap width is better defined by  $b = \frac{R_c}{\tan \theta}$ , i.e.

by assuming a paraboloid, and not a sphere, emerging tangential with the pyramidal faces, as shown in figure **Figure 1-5**. This new definition does not invalidate the original approximation but makes the solution self-consistent.

The emergence of new tip geometries becoming commercially available, such as blunted cylinders or hemispheres, makes the use of these approximate methods proposed above more and more useful. Moreover, the complexity of biological samples, requires often further corrections. In some cases, the Hertzian requirements are not fulfilled on some systems or are



too restrictive to describe the complex materials like, among others, biological samples. Several additional theoretical approaches have been formulated to overcome the limitations of Hertzian mechanics in describing more realistic systems and the most relevant to describe biological samples are summarised in the following paragraphs.

**Table 1** Principal force-indentation equations for different probe geometries

Probe geometry	Force-indentation function, $F(\delta)$	Reference	Limits of validity
Paraboloid of curvature $1/2R$ (radius $R$ )	$F = \frac{4\sqrt{R}}{3} \frac{E}{(1-\nu^2)} \delta^{\frac{3}{2}}$	(Hertz, 1881)	$\delta \ll R$
Sphere of radius $R$ and radius of contact $a$	$F = \left[ \frac{E_s}{2(1-\nu_s^2)} \left[ (a^2 + R^2) \ln \left( \frac{R+a}{R-a} \right) - 2Ra \right] \right]$ $\delta = \frac{1}{2} a \ln \left( \frac{R+a}{R-a} \right)$	(Sneddon, 1965)	$a \leq R$
Flat-ended cylinder of radius $a$	$F = 2a \frac{E}{1-\nu^2} \delta$	(Love, 1929; Rico et al., 2007; Sneddon, 1965)	$\delta \ll a$
Cone of semi-included angle $\theta$	$F = \frac{2 \tan \theta}{\pi} \frac{E}{1-\nu^2} \delta^2$	(Love, 1939; Sneddon, 1965)	$\delta \ll \tan \theta$
Blunted $n$ -sided pyramidal probe <sup>3</sup>	$F = \begin{cases} \frac{4\sqrt{R}}{3} \frac{E}{(1-\nu^2)} \delta^{\frac{3}{2}} & a < b \\ f(n, \delta, a, b) \frac{E}{(1-\nu^2)} & a > b \end{cases}$ <i>spherical cap</i> <i><math>n</math> sided regular pyramid</i> For $n = 4$ $F = \frac{\tan \theta}{\sqrt{2} \sin \left( \frac{\pi}{n} \right)} \frac{E}{1-\nu^2} \delta^2$	(Rico et al., 2005)	$h^i \ll \delta \ll 1$ $F'_{sc} = F'_p$ when $a = b$
Needle	$F = \begin{cases} F_{sphere}(\delta) & \delta \leq \delta_c \\ F_{sphere}(\delta_c) + F_{cylinder}(\delta - \delta_c) & \delta > \delta_c \end{cases}$	(Garcia and Garcia, 2018a)	$\delta \ll R$ $\delta \ll a$
Nanowire	$F = \begin{cases} F_{cone}(\delta) & \delta \leq \delta_c \\ F_{cone}(\delta_c) + F_{cylinder}(\delta - \delta_c) & \delta > \delta_c \end{cases}$	(Garcia and Garcia, 2018a)	$\delta \ll \tan \theta$ $\delta \ll a$

3

The function

$$f(n, \delta, a, b) = 2 \left( \delta a - \frac{n}{\pi} \sin \left( \frac{\pi}{n} \right) \frac{a^2}{2 \tan \theta} \left( \frac{\pi}{2} - \arcsin \frac{b}{a} \right) - \frac{a^3}{3R} + (a^2 - b^2)^{\frac{1}{2}} \left( \frac{n}{\pi} \sin \left( \frac{\pi}{n} \right) \frac{b}{2 \tan \theta} + \frac{a^2 - b^2}{3R} \right) \right)$$

,  $b = R_c \cos \theta$  for an emerging sphere or  $b = \frac{R_c}{\tan \theta}$  for an emerging paraboloid,  $h^i = \frac{b^2}{2R_c}$ , the condition

$F'_{sc}(a=b) = F'_p$  is valid when there is a smooth transition between spherical cap and pyramidal tip shape.

<b>Sphere of radius R and radius of contact a suitable also for large deformations</b>	$F = F_{Hertz} \Omega(\gamma(\delta, R))$ <p style="text-align: center;">with</p> $\Omega_{Kontomaris} = c_1 + \sum_{k=2}^6 \frac{3}{2k} c_k \gamma^{k-\frac{3}{2}}$ <p style="text-align: center;">or</p> $\Omega_{Müller} = 1 - \frac{1}{10} \gamma - \frac{1}{840} \gamma^2 - \frac{1}{15120} \gamma^3 + \frac{13}{665} \gamma^4$	(Kontomaris and Malamou, 2021a, 2021b; Müller et al., 2019)	also for $\delta > R$
--	--	--	--------------------------

### 1.3 Models considering finite sample thickness (bottom effect)

One of the Hertzian model's assumptions, as previously explained, is the infinite sample thickness, assumption number 5) in the previous section. In the case of biological samples, such as a thin lipid layers or cells, this assumption not always holds. Indeed, often in experimental conditions, cells featuring thin sections are grown on rigid substrates. In this case, when the indentation  $\delta$  cannot be considered as much smaller than the sample thickness  $h$ , the stress distribution is influenced by the presence of a stiffer substrate below the sample<sup>4</sup>. To correct for this bottom effect, advanced force-indentation relationships for different tip geometries and sample configurations have been proposed.

#### 1.3.1 Bottom effect correction for a paraboloid

A solution for this problem was proposed by Dimitriadis et al. (Dimitriadis et al., 2002) in 2002 for the case of a spherical probe or, more formally, of a paraboloid of revolution. Before Dimitriadis' model, other solutions for the bottom effect correction were formulated by Popov (Popov and Heß, 2013), Tu and Gazis (Tu and Gazis, 1964), Dhaliwal and Rau (Dhaliwal and Rau, 1970), Chen and Engel (Chen and Engel, 1972) and Aleksandrov (Aleksandrov, 1968), (Aleksandrov, 1969), but these calculations required extensive numerical computations and the Aleksandrov analytic solution is not valid for incompressible materials with Poisson's ratio  $\nu = 0.5$ . Thus, it is not suitable for biological samples which contain a large amount of water. Indeed, the difficulty of formulating a convenient approach for routine use to correct the bottom effect is due to the intrinsic nonlinearity of the problem whereby the applied total force in the  $z$  direction depends on the distribution of pressure, thus on the contact area. Dimitriadis et al. solved this issue dividing the problem of integral equations into a hierarchy of simplified subproblems, simpler integral equations that can be solved analytically, using the method of images.

In Dimitriadis' work two different cases are studied:

- the sample is not bonded to the supporting substrate
- the sample is bonded to the supporting substrate

In the first case the authors used the method of images to construct an approximate solution, while in the second case they first derived the Green's function and then used it to compute an explicit expression of the force versus indentation relationship following the same procedure as in the first case.

The method of images is based on the idea that any solution of an integral equation that satisfies the appropriate boundary conditions, like the eq (1.4), is the unique solution. The interface between the sample and the rigid substrate is considered as a singularity where the solution of the problem is unknown.

The authors assume a sample of thickness  $h$  extending in the  $x$ - $y$  plane supported on a rigid substrate located at  $z = -h$ . The force application is the same as in the Hertz model described

<sup>4</sup> As a rule of thumb, to ignore the contribution of the hard substrate, the  $\delta < 0.2h$  (Dimitriadis et al., 2002).

before, but it is assumed that the rigid boundary modifies the pressure distribution. The authors combine multiple images of the probe that apply normal forces on planes located at distances corresponding to multiples of  $2h$  from the surface of force application. Thus, an infinite number of images emerges, each representing an infinite half-space with known solution. This procedure is carried out on an infinite sequence of images.

As in the Hertz model,  $s$  is the distance between the source and the observation point,  $s=|r|=r^2+r_s^2-2rr_s\cos\phi$ . For a general image at  $z=2nh, n=0,1,2,\dots$ , the Green's function from eq (1.2) becomes here:

$$G_n(s)=i\dot{u}, \quad (1.27)$$

The total Green's function of all the images is then:

$$G_{tot}(s) = \sum_{n=0,\pm 1,\pm 2,\dots} G_n(s) \quad (1.28)$$

If we assume that the sample is not bonded to the supporting substrate, the surface in contact with the rigid substrate is free to slide horizontally, i.e. there is no friction and no adhesive contact between sample and support.

The region of interest of the original problem is only the probe contact region at the surface of the sample, accordingly we can assume that  $s \leq h$ , especially if the thickness of the sample is larger than the radius of the probe, and that the strain is small. The strain is defined as the ratio between deformation and the original height or thickness of the body in the direction parallel to the applied force. Thus, in our case we can define the parameter  $\varepsilon = \frac{\delta}{h}$ , which is small and can be regarded as a strain. At this point, we can expand the Green's function in a Taylor series in terms of  $\varepsilon$ :

$$G_{tot}(s) = G_\infty(s) \left( 1 + \varepsilon \alpha(s) + \varepsilon^3 \beta(s) + \varepsilon^5 \gamma(s) + \dots \right) \quad (1.29)$$

, where  $G_\infty(s) = \left( \frac{1-\nu^2}{\pi E} \right) \left( \frac{1}{s} \right)$  is the Green's function for the surface indentation of an infinite half-space and the higher order terms correct for the bottom effect. The coefficients of this series depend on the Poisson's Ratio *vas well*:

$$\alpha(s) = \alpha_0(\nu) \frac{s}{\delta}, \beta(s) = \beta_0(\nu) \left( \frac{s}{\delta} \right)^3, \gamma(s) = \gamma_0(\nu) \left( \frac{s}{\delta} \right)^5, \dots \quad (1.30)$$

The expressions of the coefficients  $\alpha_0(\nu), \beta_0(\nu)$  and  $\gamma_0(\nu)$  can be found in the original work by Dimitriadis et al. (Dimitriadis et al., 2002).

Since the probe is spherical and we assume negligible long-range interactions, the displacement field will follow the shape of the probe and eq. (1.4) becomes:

$$\delta - \frac{r^2}{2R} = \iint_A P(r_s) G_{tot}(s) dA \quad (1.31)$$

where the Green's function  $G_{tot}(s)$  is given by eq. (1.29) The contact area and accordingly the contact radius are assumed to be independent of  $h$ , because the radius of the probe is smaller than the sample thickness. Thus, the presence of the rigid substrate modifies the pressure

profile without affecting the contact area. It is then reasonable that the pressure profile depends on the small parameter  $\varepsilon$  and expand it in Taylor series as before for  $G_{\text{tot}}$ :

$$P(r_s) = P_\infty(r_s) \left( 1 + \varepsilon \alpha(s) + \varepsilon^3 \beta(s) + \varepsilon^5 \gamma(s) + \dots \right) \quad (1.32)$$

Through the substitution of eq. (1.28) in eq. (1.27) we obtain a series of integral equations of different order for  $P_\infty, P_1, P_2, P_3$  etc. Each order problem can be solved separately. The first order problem solution is exactly the Hertz model of a rigid spherical probe indenting an infinite half-space (eq. (1.10)). Calculating the solutions of the integral equations until fourth order the expression of the force in a function for the indentation of a spherical probe indenting an infinite half-space multiplied with a series of terms correcting for the finite thickness or bottom effect:

$$F = \frac{4\sqrt{R}}{3} \frac{E}{(1-\nu^2)} \delta^{\frac{3}{2}} \left[ 1 - \frac{2\alpha_0}{\pi} \chi + \frac{4\alpha_0^2}{\pi^2} \chi^2 - \frac{8}{\pi^3} \left( \alpha_0^3 + \frac{4\pi^2}{15} \beta_0 \right) \chi^3 + \frac{16}{\pi^4} \left( \alpha_0^4 + \frac{3\pi^2}{5} \beta_0 \alpha_0 \right) \chi^4 \right] \quad (1.33)$$

where  $\chi = \frac{a}{h} = \sqrt{R\delta}/h$ .

Eq. (1.33) is the finite thickness solution for a parabolic probe (which also closely approximates a spherical probe) valid whether the sample is bonded to the substrate or not. The difference between the two cases consists in the parameters  $\alpha_0$  and  $\beta_0$ , which depend differently on the Poisson's ratio  $\nu$  in these two cases.

Noticeably, the bottom effect correction does not depend trivially on the ratio of the vertical lengths  $\delta$  and  $h$ , but rather on the ratio of the horizontal dimension of the contact, the contact radius  $a$ , to the sample height  $h$ . The correction therefore considers the propagation of the strain and stress fields into the bulk volume of the sample, not only their vertical extension. Therefore, we must expect stronger finite-thickness effects for large spherical-parabolic probe with respect to sharp ones.

For most biological samples, we can assume  $\nu=0.5$ . In this case the equations for bonded and not bonded samples become:

Sample not bonded:

$$F = \frac{16\sqrt{R}E}{9} \delta^{\frac{3}{2}} [1 + 0.884 \chi + 0.781 \chi^2 + 0.386 \chi^3 + 0.0048 \chi^4], \quad (1.34)$$

Sample bonded:



$$F = \frac{16\sqrt{R}E}{9} \delta^{\frac{3}{2}} [1 + 1.133\chi + 1.283\chi^2 + 0.769\chi^3 + 0.0975\chi^4]. \quad (1.35)$$

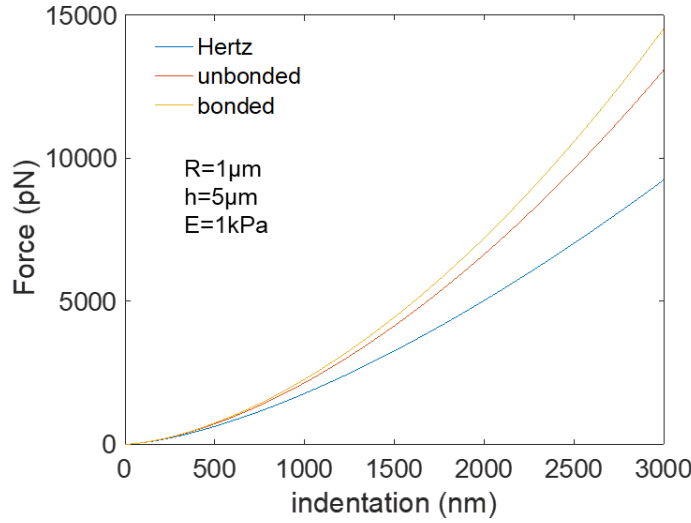


**Figure 1-6** Force-indentation curve of Bottom effect model in the case of sample bonded and unbonded in comparison with the Hertz model for a parabolic indenter with curvature radius  $R = 1 \mu\text{m}$ , sample thickness  $h = 5 \mu\text{m}$  and Young's Modulus  $E = 1\text{kPa}$ .

The curves corresponding to these bottom-corrected equations are shown in figure Figure 1-6 and compared with the Hertz model. When comparing these two equations, the apparent stiffness of the sample is larger for the bonded case, which coincides with intuition since the sample is not allowed to slide laterally.

For the intermediate case, in which only some parts of the sample are bonded, we can replace eq. (1.34) and eq. (1.35) with a similar equation in which the numerical coefficients are the average of the corresponding coefficients in the two cases; this can be appropriate for cells, which adhere locally to a substrate through dynamically forming focal adhesion complexes (Gavara and Chadwick, 2012).

Clearly, for any given tip radius, there is a limited range of thickness and indentation for which eq.1.30 and eq.1.31 are valid. In order to respect the assumption of linear elasticity of the material, the maximum total strain should never exceed 10%, or  $\delta \leq 0.1h$ . We can consider that the bottom effect correction is required if the first term of the series adds at least to 10% of the force. For the bonded case, this means that  $1.133\chi \geq 0.1$  with  $\chi = \sqrt{R\delta}/h$ , which implies  $h \leq 12.83R$ . Thus, for sample thickness with  $h > 13R$  the infinite half-space assumption can be considered a good approximation.

At the same time, to use safely this model,  $h$  cannot be much smaller than  $R$ . Indeed, the parameter  $\chi$  of this series has to be small enough. If  $\chi$  is too large, the series expansion may lose accuracy and could diverge. The series converges if  $\chi \leq 1$ , which implies  $h \geq 0.1R$ .

The previous formulation assumes Hertzian contact area ( $a = \sqrt{R\delta}$ ), which is not necessarily given. Imposing that the contact area at each indentation point follows  $\frac{\partial F(\delta, a)}{\partial a} = 0$ , Garcia

and Garcia (Garcia and Garcia, 2018a) found that the equivalent of eq.

$$F = \frac{16\sqrt{R}E}{9} \delta^{\frac{3}{2}} [1 + 0.884\chi + 0.781\chi^2 + 0.386\chi^3 + 0.0048\chi^4], \quad (1.34)$$

for a bonded sample presents slightly different correction terms:

$$F = \frac{16\sqrt{R}E}{9} \delta^{\frac{3}{2}} [1 + 1.133\chi + 1.497\chi^2 + 1.469\chi^3 + 0.755\chi^4]. \quad (1.36)$$

which imposes a stronger correction.

If the sample is very thin,  $h \leq 0.1R$ , these models do not describe the physics of the problem, and the following formulas obtained in Chadwick et al. (Chadwick, 2002) should be used.

Sample not bonded:

$$F = \left(\frac{2\pi}{3}\right) E \sqrt{R\delta^3} \chi^3 \quad (1.37)$$

Sample bonded:

$$F = \left(\frac{2\pi}{3}\right) E \sqrt{R\delta^3} \chi^3 \quad (1.38)$$

In conclusion, the bottom effect correction is necessary to avoid an overestimation of the Young's Modulus when the sample thickness is not infinite. If the sample is too thin compared to the radius, approximately  $h \leq 13R$  (Dimitriadis et al., 2002), the rigid substrate blocks the propagation of the stress field induced by the tip in the sample. This phenomenon affects the distribution of the pressure and decreases the deformation of the sample, with a consequent increase of the apparent Young's Modulus  $E$ .

It should also be noted that the bottom effect correction allows to consider in the analysis also those thinner regions of the sample (like the peripheral extensions and lamellipodia in the cells) where usually the estimation of the Young's modulus is poorly accurate.

Besides the vertical spatial constraint represented by the substrate supporting the system under study, it can be assumed that also lateral confinement and boundaries produce similar effects, for which analytical corrections are not available but only FEM simulations (Garcia and Garcia, 2018, supplement material). This can be relevant, for example, for the nanomechanical characterisation of cells in a confluent layer, where strong cell-cell interactions determine lateral boundaries, which can interfere with the strain field induced by the indenter, especially when large spherical probes are used.

### 1.3.2 Bottom effect correction for other geometries

In case of other tip geometries, like conical and pyramidal, the pressure distribution  $P(r)$  for the bottom effect correction can be approximated, as explained before, knowing the expression of the work  $F\delta$  for a flat cylinder probe and using Betti's reciprocal theorem and then the Rayleigh-Ritz approximation. Then, the pressure distribution can be computed using the integral equation:

$$\delta = \iint_A P(r) G_{tot}(s) dA \quad (1.39)$$

Using the Green's function described above for finally finding the force as a function of the contact radius. Finally, the contact radius can be found by imposing again  $\frac{\partial F}{\partial a} = 0$ . The full development to correct the bottom effect of a bonded sample of finite thickness for a conical probe was formulated in the work of Gavara and Chadwick (Gavara, 2016). However,

according to later works the solution provided was not convergent, probably due to a typographical error (Garcia and Garcia, 2018a; Managuli and Roy, 2018). Following the same approach, slightly different factors were found, which lead to a convergent series of the force  $F$  (more details in the supplementary materials of Garcia and Garcia, 2018). We provide here the solution reported by Garcia and Garcia.

$$F = \frac{8 \tan \theta}{3 \pi} E \delta^2 \left[ 1 + 0.721 \tan \theta \frac{\delta}{h} + 0.650 \tan^2 \theta \left( \frac{\delta}{h} \right)^2 + 0.491 \tan^3 \theta \left( \frac{\delta}{h} \right)^3 + 0.225 \tan^4 \theta \left( \frac{\delta}{h} \right)^4 + O \left( \left( \frac{\delta}{h} \right)^5 \right) \right] \quad (1.40)$$

Following the same approach, Garcia and Garcia also reported the solutions for a paraboloid, extending the solution for the case of non Hertzian contact radius, and for a flat-ended cylinder of radius  $a$ . Interestingly, for a flat ended cylinder, the force-indentation relationship remains linear for finite sample thicknesses. The principal force-indentation solutions for bottom effect correction for different geometrical probe models are shown in Table 2. Other solutions for the indentation of different probe geometries indenting thin samples, with their own limitations, can be found in the literature (Akhremitchev and Walker, 1999; Long et al., 2011; Yang, 1998).

Recent developments have established the use of soft substrates for cell culture. In that case, a bottom effect correction may be needed to prevent underestimation of cell mechanics. Solutions have been provided for the case of two layered elastic substrates, which might be important for accurate estimation of the Young's modulus of living cells growing on soft hydrogels (Doss et al., 2019). In the case of a thin sample with Young's Modulus  $E_1$ , placed on a softer substrate with Young's Modulus  $E_2$ , where  $E_1 > E_2$ , the force-indentation relation is described by the following equation, obtained by Doss et al.:

$$F = \frac{16 \sqrt{R} E_1}{9} \delta^{\frac{3}{2}} \left( \frac{0.85 \chi + 3.36 \chi^2 + 1}{\left( 0.85 \chi + 3.36 \chi^2 \right) \left( \frac{E_1}{E_2} \right)^{0.72 - 0.34 \chi + 0.51 \chi^2} + 1} \right) \quad (1.41)$$

Recently, Rheinlaender et al. proposed a model for the indentation of a living cell on a soft substrate. The model assumes a uniform deformation of the cell contact area and was validated for the case of large spherical tips, which causes not only an indentation of the cell but also a coupled indentation of the soft substrate ( $R \gg h_{cell}$ ) (Rheinlaender et al., 2020).

**Table 2:** Principal force-indentation equations for the bottom effect corrected models for different probe geometries

Probe geometry	Force-indentation function, $F(\delta)$	Reference	Limits of validity
Paraboloid of curvature $1/2R$	$F = \frac{16 \sqrt{R} E}{9} \delta^{\frac{3}{2}} [1 + 0.884 \chi + 0.781 \chi^2 + 0.386 \chi^3 + 0.0048 \chi^4]$	(Dimitriadis et al., 2002)	$\chi = \sqrt{R\delta}/h \ll 1$

<sup>5</sup> The difference of the needle and nanowire models between Table 1 and Table 2 is that in Table 1  $F_{sphere}$ ,  $F_{cylinder}$  and  $F_{cone}$  are not bottom effect corrected, while in Table 2 they are corrected for the bottom effect thanks to the multiplication with the Taylor series coefficient. Moreover, we added to this table two models for a paraboloidal probe by Dimitriadis et al and Garcia et al. because both are valid models, but they present some differences: the Gracia et al model is valid when the paraboloid is closer to a sphere and the force values are higher vs time than Dimitriadis et al model, if the same parameters are used, this is very well explained in the supplementary materials of Garcia and Garcia, 2018.

<b>(radius R) Sample not bonded</b>			
<b>Paraboloid of curvature 1/2R (radius R) Sample bonded</b>	$F = \frac{16\sqrt{R}E}{9} \delta^{\frac{3}{2}} [1 + 1.133 \chi + 1.283 \chi^2 + 0.769 \chi^3 + 0.0975 \chi^4]$	(Dimitriadis et al., 2002)	$\chi = \sqrt{R\delta}/h \ll 1$
<b>Cone of semi-included angle <math>\theta</math> or pyramid</b>	$F = \frac{8 \tan \theta E}{3\pi} \delta^{\frac{3}{2}} [1 + 0.721 \tan \theta \chi + 0.650 \tan^2 \theta \chi^2 + 0.491 \tan^3 \theta \chi^3]$	(Garcia and Garcia, 2018a; Gavara and Chadwick, 2012)	$\chi = \frac{\delta}{h} \ll 1$
<b>Sphere (Paraboloid very close to a Sphere of radius R)</b>	$F = \frac{16\sqrt{R}E}{9} \delta^{\frac{3}{2}} [1 + 1.133 \chi + 1.497 \chi^2 + 1.469 \chi^3 + 0.755 \chi^4]$	(Garcia and Garcia, 2018a)	$\chi = \frac{\sqrt{R\delta}}{h} \ll 1$ $\delta \ll R$
<b>Flat-ended cylinder of radius a</b>	$F = \frac{8aE}{3} \delta [1 + 1.133 \chi + 1.283 \chi^2 + 0.598 \chi^3 + 0.291 \chi^4]$	(Garcia and Garcia, 2018a)	$\chi = \frac{a}{h} \ll 1$
<b>Needle</b>	$F = \begin{cases} F_{sphere}(\delta) & \delta \leq \delta_c \\ F_{sphere}(\delta_c) + F_{cylinder}(\delta - \delta_c) & \delta > \delta_c \end{cases}$	(Garcia and Garcia, 2018a)	$\frac{\sqrt{R\delta}}{h} \ll 1$ $\frac{a}{h} \ll 1$ $\delta \ll R$
<b>Nanowire</b>	$F = \begin{cases} F_{cone}(\delta) & \delta \leq \delta_c \\ F_{cone}(\delta_c) + F_{cylinder}(\delta - \delta_c) & \delta > \delta_c \end{cases}$	(Garcia and Garcia, 2018a)	$\frac{a}{h} \ll 1$ $\delta/h \ll 1$
<b>Paraboloid of curvature 1/2R (radius R) Layered soft elastic substrate</b>	$F = \frac{16\sqrt{R}E_1}{9} \delta^{\frac{3}{2}} \left( \frac{0.85 \chi + 3.36 \chi^2 + 1}{(0.85 \chi + 3.36 \chi^2) \left( \frac{E_1}{E_2} \right)^{0.72 - 0.34 \chi + 0.51 \chi^2} + 1} \right)$	(Doss et al., 2019)	$\chi = \sqrt{R\delta}/h \ll 1$ $E_1 > E_2$

## 1.4 Viscoelastic models

Living cells have a viscous, liquid-like component, and an elastic, solid-like component, both coupled and arising from the complex filament network of the cytoskeleton within the cytosol (Fabry et al., 2001; Rigato et al., 2017). Thus, cells are viscoelastic, and such are many other systems that can be studied by AFM or other indenters. When a force is applied on a purely elastic material, there is not dissipation of energy and the response to the force is instantaneous. On the contrary, when the sample is viscoelastic, there is a loss of energy inside the material and the response of the sample to the external stimulus is delayed. Therefore, viscoelasticity is a time-dependent anelastic behaviour of materials.

The viscoelastic response of complex systems such as cells or tissues, formed of different types of polymers, often occurs over a wide range of time scales and comprises a continuum of relaxation times. Dissipative stresses inside the material can be due to the structure and

mechanical properties of the polymeric network, but may also be an effect of the flow of liquid through the porous matrix (Moeendarbary et al., 2013; Kalcioğlu et al., 2012).

Unlike purely elastic materials that recover their shape after the applied load is removed and unlike purely viscous materials that remain in the deformed state after the applied load is removed, viscoelastic materials present a superposition of these two properties. Such a behaviour may be linear (stress and strain are proportional) or nonlinear. We will only consider the linear viscoelastic regime. Viscoelasticity is observed as a combination of both recoverable elastic and permanent viscous deformation. Nearly all biopolymers solutions, cells and biological tissues, exhibit viscoelasticity.

So far, we have been focusing on the approach curve to fit the contact elastic models. This may be partially due to a historical choice motivated by the fact that the retraction curve often features adhesion events that may affect the fitting procedure and the final results (Radmacher et al., 1996). In addition to the presence of adhesive features, as observed in fig. Figure 1-1, the approach and retract curve may not coincide, being the force in the retract trace typically lower. Excluding the presence of plastic deformations, which is reasonable for relatively small indentations, this reflects some kind of dissipation during the whole cycle, likely due to the viscoelastic nature of cells. Indeed, the opening of the approaching-retracting force curve loop typically increases as the ramping frequency increases. Different types of approaches can be applied to determine the dynamic response of materials. Mainly, oscillatory experiments (an oscillatory strain or stress is applied and the resulting stress or strain, respectively, is measured) at constant frequency or sweeping through a frequency range, and creep experiments (a stress is applied and kept constant, while strain over time is measured) or relaxation experiments (a strain is applied and kept constant, while the stress over time is measured) (Alcaraz et al., 2003; Mahaffy et al., 2000). In this section, we will focus on recent solutions describing the shape of force-distance curves on a viscoelastic material. Recent AFM applications of theoretical developments have led to a set of equations that allow complete fit of the loading and unloading force curves (or approach and retract) taking into account a viscoelastic response of the sample.

There are various approaches to determine the viscoelastic force-indentation relationship of a viscoelastic sample, some using numerical integration and others analytical approximations, all based on the seminal works by Lee and Radock, Graham and Ting (Brückner et al., 2017; D. Garcia et al., 2020; Efremov et al., 2017, 2020; Graham, 1965; Lee and Radok, 1960; Ting, 1966). We will follow here the approach recently reported by Brückner and co-workers, which provides an analytical solution assuming constant indentation velocity and power law rheology. The general approach requires solving two problems, one for the loading part and one for the unloading. Brückner and co-workers assume a linear indentation ramp that leads to a maximum in the contact radius upon loading, and then decreases upon unloading. The solution uses equivalent elastic contact mechanics with the elastic modulus being a function of the loading history. Thus, it requires the definition of the viscoelastic response of the sample. As shown before for a number of cell types and tissues, using AFM and other techniques, the viscoelasticity of living cells and extracellular matrices is well described by a power law relaxation function,  $E(t) = E_0 \Psi(t) = E_0 (t/t_0)^{-\beta}$ , both at low and at high frequencies (Balland et al., 2006; Fabry et al., 2001; Jorba et al., 2017; Rigato et al., 2017). Thus, we will limit our description to the solution of a material exhibiting such a power law response. While solutions have been proposed for other viscoelastic relaxation functions  $\Psi(t)$ , such as standard linear solid or Kelvin-Voigt models, their application to living cells is limited (Garcia, 2020; Garcia and Garcia, 2018; Greenwood et al., 1966).

All proposed approaches depart from the definition of time dependent force ( $F(t)$ ) that, in turns, depend on the time-dependent Young's modulus ( $E(t)$ )

$$F(t) = \tilde{C}^{-1} \int_0^t E(t-\tau) \frac{\partial \delta(t)^n}{\partial \tau} d\tau \quad (1.42)$$

where  $E(t) = E_0 \psi(t-\tau)$ , with  $\psi$  being the relaxation function describing the viscoelastic response of the material,  $\delta$  is the indentation and the pre-factor  $\tilde{C}$  and the exponent  $n$  are constants that depend on the tip geometry as defined below, actually they are given by the force and indentation in the equivalent contact elastic model (e.g.  $n=2$  for a cone,  $n=3/2$  for a paraboloid of revolution).

To determine the prefactor  $\tilde{C}$  and the indentation, Brückner et al. (Brückner et al., 2017), the authors use the approach by Popov for an arbitrary axisymmetric punch of profile  $f(r)$ , that relates the indentation up to a time  $t=t_m$  (time of maximum contact radius  $a(t_m)=a_{\max}$ ) with the time depending contact radius (Popov, 2010)

$$\delta(t) = a(t) \int_0^{a(t)} \frac{f'(r) dr}{\sqrt{a^2(t) - r^2}} \quad (1.43)$$

This assumes a monotonically increasing contact radius, which is achieved for the case of a linear indentation ramp  $\delta(t) = v_0 t$ . Then, the force is given by

$$F(t) = 2 E_0 \int_0^t \psi(t-\tau) \frac{\partial}{\partial \tau} \left( \int_0^{a(\tau)} \frac{f'(r) r^2 dr}{\sqrt{a^2(\tau) - r^2}} \right) d\tau \quad (1.44)$$

The indentation profiles for a cone, a paraboloid and a flat cylinder have been defined above. For a cone

$$\delta(t) = \left( \frac{\pi}{2} \right) a(t) \cot \alpha, \tilde{C}_c = \frac{\pi(1-v^2)}{2 \tan \alpha} \wedge n=2 \quad (1.45)$$

for a paraboloid of revolution

$$\delta(t) = \left( \frac{a^2(t)}{R} \right), \tilde{C}_p = \frac{3(1-v^2)}{4\sqrt{R}}, \wedge n = \frac{3}{2}, \quad (1.46)$$

and for a flat-ended cylinder of radius  $a_{cp}$  the indentation does not depend on the contact radius and therefore we can simply use  $\tilde{C}_{cp} = \frac{1-v^2}{2 a_{cp}}$ .

In principle, the loading trace can be generalized for a non-axisymmetric punch by defining the appropriate punch profile depending also on the azimuthal angle  $f(r)$  and using the Rayleigh-Ritz approximation of the contact area (see above). Although not rigorously developed, the symmetry of the problem suggests a possible approximation using such an approach. Indeed, in the work of Brückner and co-workers, the authors assumed that for a regular 4-sided pyramid, the final solution will be the same as for a cone, but with a different

geometrical pre-factor  $\delta(t) = \sqrt{2} a(t) \cot \alpha$ , and  $C = 1.342 \frac{1-v^2}{\tan \alpha}$  obtained from the numerical

solution by Bilodeau, or  $\tilde{C}_{pyr} = \frac{\sqrt{2}(1-v^2)}{\tan \alpha}$  from the analytical approximation by Barber and

Billings (Barber and Billings, 1990; Bilodeau, 1992).

As mentioned before, the relaxation function is assumed to follow a power law response with

$\psi(t) = \left(\frac{t}{t_0}\right)^{-\beta}$ , i.e.  $E(t) = E_0 \left(\frac{t}{t_0}\right)^{-\beta}$ . Thus, from eq. 1.41, for the loading or approach trace<sup>6</sup> for a

cone, they obtain

$$F_a(t) = \frac{v_0^2}{\tilde{C}_c} \int_0^t E_0 \left(\frac{t-\tau}{t_0}\right)^{-\beta} \tau d\tau = 2 \frac{v_0^2}{\tilde{C}_c} E_0 \frac{t_0^\beta}{(2-3\beta+\beta^2)} t^{2-\beta} = 2 \frac{v_0^2}{\tilde{C}_c} E_0 \frac{t_0^\beta \Gamma[2] \Gamma[1-\beta]}{\Gamma[3-\beta]} t^{2-\beta} = 2 \frac{E(t)}{\tilde{C}_c (2-3\beta+\beta^2)} \delta^2(t) \quad (1.47)$$

For a paraboloid

$$F_a(t) = \frac{v_0^{\frac{3}{2}}}{\tilde{C}_p} \int_0^t E_0 \left(\frac{t-\tau}{t_0}\right)^{-\beta} \tau^{1/2} d\tau = \frac{v_0^{\frac{3}{2}}}{\tilde{C}_p} E_0 \frac{t_0^\beta 3\sqrt{\pi} \Gamma(1-\beta)}{4 \Gamma\left(\frac{5}{2}-\beta\right)} t^{\frac{3}{2}-\beta} = \frac{3 E(t) \sqrt{\pi} \Gamma(1-\beta)}{\tilde{C}_p 4 \Gamma\left(\frac{5}{2}-\beta\right)} \delta^{3/2}(t) \quad (1.48)$$

And for a flat-ended cylinder

$$F_a(t) = \frac{v_0}{\tilde{C}_{cp}} \int_0^t E_0 \left(\frac{t-\tau}{t_0}\right)^{-\beta} d\tau = \frac{v_0}{\tilde{C}_{cp}} E_0 \frac{t_0^\beta}{(1-\beta)} t^{1-\beta} = \frac{E(t)}{\tilde{C}_{cp} (1-\beta)} \delta(t) \quad (1.49)$$

Calculation of the unloading trace requires knowledge of the time  $t_1 < t_m$  at which  $a(t) = a(t_1)$  for  $t > t_m$ . Again, assuming unloading with a linear indentation ramp at the same rate than during loading, going from  $t_m$  until  $\delta(t) = 0$ . Thus, the indentation follows  $\delta(t) = v_0(2t_m - t)$  and the contact radius decreases monotonically for  $t > t_m$  from the maximum at  $t = t_m$ .

With the condition to find  $t_1(t)$  being

$$\int_{t_1(t)}^t \psi(t-\tau) \frac{\partial \delta(t)}{\partial \tau} d\tau = 0 \quad (1.50)$$

And substituting the form of  $\delta(t)$  and solving  $\Psi(t) = \left(\frac{t}{t_0}\right)^{-\beta}$  leads to

---

<sup>6</sup> In the loading or approach trace equations the expression  $\frac{\Gamma[2] \Gamma[1-\beta]}{\Gamma[3-\beta]} = 1/(2-3\beta+\beta^2)$ , the same also for the unloading or retract trace equations.

$$t_1(t) = t - 2^{\frac{1}{1-\beta}}(t - t_m) \quad (1.51)$$

A relevant assumption of this approach is that the contact area increases monotonically with time, which is important for using Lee and Radok's viscoelastic correspondence principle (Lee and Radok, 1960). Thus, as developed by Ting, the retract trace is derived from the approach elastic solution with increasing contact area eq 1.44, but with the integration going from 0 to  $t_1(t)$ . Thus, for a cone, we obtain

$$F_r(t) = 2 \frac{v_0^2 E_0 t_0^\beta}{\widetilde{C}_c (2 - 3\beta + \beta^2)} \left( 2 \left[ t(2 - \beta) + 2^{\frac{1}{1-\beta}} (1 - \beta)(t - t_m) \right] (t - t_m)^{1-\beta} - t^{2-\beta} \right) \quad (1.52)$$

For a paraboloid, the retract expression would involve ordinary hypergeometric functions ( ${}_2F_1$ )

$$F_r(t) = \frac{3v_0^{\frac{3}{2}} E_0 t_0^\beta}{\widetilde{C}_p (3 + 4(\beta - 2)\beta)} t_1^{-1/2} (t - t_1)^{1-\beta} \left( (2\beta - 1)t_1 - t + {}_2F_1 \left( 1, \frac{1}{2} - \beta, \frac{1}{2}, \frac{t_1}{t} \right) \right) \quad (1.53)$$

And for a flat-ended cylinder

$$F_r(t) = \frac{v_0}{\widetilde{C}_{cp}} E_0 \frac{t_0^\beta}{(1 - \beta)} \left( t^{1-\beta} - 2(t - t_m)^{1-\beta} \right) \quad (1.54)$$

As noticed by Ting, the contact radius is given by the indenter shape during loading, but it also depends on the material properties during unloading.

The loading and unloading trace equations for the viscoelastic model obtained by Brückner et al. are recapitulated in Table 3. In principle, the above approach should be also valid for the case of different loading and unloading velocities. As mentioned before, the developed models assume a linear indentation ramp. This is an important assumption. This condition was verified by the authors in AFM measurements on cells, concluding that it will be valid when applying a linear piezo ramp using relatively stiff cantilevers to indent a soft sample. More practically, the assumption is valid if the deflection of the cantilever is negligible compared to the applied indentation. If the linear indentation rate assumption does not hold, numerical approaches have been proposed by Efremov and co-workers including corrections for the bottom effect (Efremov et al., 2017, 2020) based on the above equations for  $F(t)$  and  $t_1(t)$  (eq. (1.47) and eq. (1.51)). An analytical approximation for a viscoelastic sample of finite thickness was also recently reported by Garcia and co-workers (Garcia, 2020) as introduced in the next section.

In Table 3,  $\widetilde{C}_p = \frac{3(1-v^2)}{4\sqrt{R}}$ , for a paraboloid,  $\widetilde{C}_c = \frac{\pi(1-v^2)}{2 \tan \alpha}$  for a cone  $\widetilde{C}_{pyr} = \frac{\sqrt{2}(1-v^2)}{\tan \alpha}$  for a pyramid,  $\widetilde{C}_{cp} = \frac{1-v^2}{2a_{cp}}$  for a flat cylinder.



**Table 3<sup>7</sup>** Principal force-time equations for the viscoelastic models for different probe geometries, where  $F(t)$  is the approach curve and  $F_b(t)$  the retract

Probe geometry	Force-time function, $F(t)$	Reference	Limits of validity
<b>Cone of semi-included angle <math>\theta</math> or pyramid</b>	$F_a(t) = \frac{2}{\widetilde{C}_c \sqrt{\widetilde{C}_{pyr}}} \frac{v_0^2 E_0 t_0^\beta}{\widetilde{C}_c (2-3\beta+\beta^2)} t^{2-\beta}$ $F_r(t) = \frac{2}{\widetilde{C}_c \sqrt{\widetilde{C}_{pyr}}} \frac{v_0^2 E_0 t_0^\beta}{(2-3\beta+\beta^2)} \left( 2 \left[ t(2-\beta) + 2^{\frac{1}{1-\beta}} (1-\beta) \right] \right)$	(Brückner et al., 2017)	Linear, equal approach and retract $\delta(t)$
<b>Paraboloid of curvature 1/2R (radius R)</b>	$F_a(t) = \frac{v_0^{3/2}}{\widetilde{C}_p} E_0 \frac{t_0^\beta 3\sqrt{\pi} \Gamma(1-\beta)}{4 \Gamma\left(\frac{5}{2}-\beta\right)} t^{\frac{3}{2}-\beta}$ $F_r(t) = \frac{3v_0^{\frac{3}{2}} E_0 t_0^\beta}{\widetilde{C}_p (3+4(\beta-2)\beta)} t_1^{-1/2} (t-t_1)^{1-\beta} \left( (2\beta-1)t_1 - t + \dots \right)$	(Brückner et al., 2017) and this chapter	Linear, equal approach and retract $\delta(t)$
<b>Flat-ended cylinder of radius <math>a</math></b>	$F_a(t) = \frac{v_0}{\widetilde{C}_{cp}} E_0 \frac{t_0^\beta}{(1-\beta)} t^{1-\beta}$ $F_r(t) = \frac{v_0}{\widetilde{C}_{cp}} E_0 \frac{t_0^\beta}{(1-\beta)} \left( t^{1-\beta} - 2(t-t_m)^{1-\beta} \right)$	(Brückner et al., 2017) and this chapter	Linear, equal approach and retract $\delta(t)$

### 1.5 Bottom effect correction for viscoelastic models

In the previous sections we have seen the importance of probe geometry, sample thickness and sample viscoelasticity when mechanical properties of soft materials are to be obtained from force-distance curves. The contact models explained above consider different probe geometries, sample finite thickness and sample viscoelasticity. Both living tissues and cells are viscoelastic, as mentioned before, but while tissues are generally thick compared to the indentation achieved during nanomechanical measurements, living cells can instead be very thin and a bottom effect correction is often needed. Therefore, accurate determination of cell mechanics across the whole cell surface requires combining a viscoelastic model with a bottom-effect correction for different probe geometries, to consider at the same time the finite thickness of the cell and its complex viscoelastic response. Different approaches have been proposed before (Darling et al., 2007).

A simple and practical analytical solution was proposed by (Garcia and Garcia, 2018b). In this model, the cell was considered as an incompressible material with a linear viscoelastic response described by a Kelvin-Voigt model. The authors later realized that the Kelvin-Voigt model lead to an artefactual jump in the retraction curve, not observed experimentally in living cells and proposed the solution for a power law model (Garcia, 2020). Thus, only the model derived from the power law relaxation function is valid in both loading and unloading traces for living cells. The universal power law response observed in living cells further justifies this choice (Fabry et al., 2001).

<sup>7</sup> We prefer to present in this table the force-time instead of the force-indentation equations, because the viscoelastic model depends on time, as explained before, so it is easier to obtain the analytical expression of force in function of time from the theory. The conversion from a force-time curve to a force-indentation curve is straightforward when it is known the waveform that describe the tip-sample distance  $\delta(t)$ .

The proposed development is based on:

- 1) Betti's reciprocal theorem and Rayleigh-Ritz approximation to relate pressures and deformations for different geometries
- 2) The equivalence principle between elastic and viscoelastic deformation
- 3) Ting's method to obtain the force as a function of deformation history
- 4) Boundary conditions involving a cell adherent on a rigid support

The authors provide analytical solutions for a conical indenter and we refer to the original article for the specific equations (Garcia, 2020).

We have provided relevant contact models to quantify the mechanics of soft, complex systems from AFM force-distance curves focusing on the importance of probe geometry, sample thickness and energy dissipation. One of the parameters that we have ignored and might be relevant is adhesion. This will be briefly addressed in the following section.

## 1.6 Contact models considering adhesion

As mentioned above, the dissipative response of biomaterials, reflected by hysteresis between loading and unloading curves, is often due to the viscoelastic response of the sample. However, adhesion between the probe and the sample may also be at the origin. Indeed, when working with cells or tissues, adhesion between the AFM tip and the sample is often observed and tip passivation strategies can be used to minimize it.

On some occasions, probes are functionalized with adhesion proteins to measure adhesion or non-specific adhesion which occur between the tip and the sample. In that case, the force-distance curves will feature pronounced negative forces upon unloading due to the stretching of the sample through the formed bonds. The analysis of this type of curves is generally not carried out using continuum contact elastic models considering adhesion and might not be convenient for measurements on cells or tissues, as adhesion is often mediated by discrete adhesion complexes not well described by the formalism required in continuum mechanics. Instead, non-specific adhesion on macroscopic objects is more prone to this type of analysis. Nevertheless, it might be useful to know the available models developed in the context of classical non-specific adhesion on macroscopic objects. Moreover, some commercial softwares use such models. We thus briefly describe here the most known JKR and DMT contact models, since they may help in better estimating the sample elastic modulus under conditions of adhesion.

After the initial work by Derjaguin (Derjaguin, 1934), the first approaches to adhesion between elastic bodies in contact were developed by Johnson, Kendall and Roberts (the JKR model), and by Derjaguin, Muller and Toporov (the DMT model) (Derjaguin, 1934; Johnson, 1985). Tabor discussed the transition from the DMT to the JKR regime (Tabor, 1977), while Maugis developed a generalised multiparametric model (Maugis, 1992; Popov, 2010).

When considering adhesion between two elastic bodies, unlike the developments explained before, in addition to compression stresses we should consider tensile traction, mainly generated both outside or inside the contact area, depending on the adhesive properties of the interacting surfaces and on the size of the contact region. Thus, at zero applied force, the contact area is not zero, but finite.

In this section, we will present two of the most used models: JKR and DMT (Derjaguin et al., 1975; Johnson et al., 1971). In general, JKR is valid for large, flexible spheres and short-range adhesive interactions; under these conditions, the leading contribution to adhesion comes from inside the contact area, and it therefore depends on the applied load. DMT is typically valid for small, rigid surfaces in contact (or at least one of the two) and/or long-ranged adhesive interactions; under these conditions, the contribution to adhesion from outside the contact area is dominating, and nearly constant (Popov et al., 2019a). Both models consider a

spherical indenter of radius  $R$  in contact with a planar surface. Often the models are presented with the sphere being the elastic body, while the surface is rigid, but the formulation is valid for the opposite case, too.

The JKR assumes that the energy of the interaction is given by an elastic, storage term described by the Young's modulus ( $E$ ), and an attractive, dissipative term described by a surface energy ( $\gamma$ )<sup>8</sup> acting only within the contact area (Johnson, 1985). The pressure distribution in the contact area is then assumed to be a superposition of the Hertzian pressure due to compressive stresses of the elastic body around the center and the flat cylinder pressure due to tensile stresses (diverging at the rim of contact) given by the presence of adhesion forces. By considering the work done in compression by the pressure and minimizing the total energy at equilibrium, it was found that in the JKR model, there still exist a formally Hertzian relationship between the contact radius  $a$  and an effective force  $F_{JKR}$ , which takes adhesion into account:

$$F_{JKR} = \frac{4}{3} \frac{E^{\dot{c}}}{R} a^3 \quad (1.55)$$

with

$$F_{JKR} = F_n + 6\pi\gamma R + \sqrt{12\pi\gamma R F_n + (6\pi\gamma R)^2} \quad (1.56)$$

where  $F_n$  is the external applied force,  $E^{\dot{c}} = \frac{E}{1-\nu^2}$  is the reduced Young's modulus.

Solving for  $F_n$  provides a relation between  $F_n$  and the contact radius  $a$

$$F_n = E^{\dot{c}} \left( \frac{4}{3} \frac{a^3}{R} - 4 \sqrt{\frac{\pi\gamma a^3}{E^{\dot{c}}}} \right) \quad (1.57)$$

Notice that the first term in eq. (1.57) reminds of the Hertz model, but with a larger contact radius. The second term accounts for the force due to adhesion and depends on the rigidity of the sample (the softer the sample, the larger the contact area, the higher the adhesive force). Because of adhesion forces, the same contact radius can be obtained with a smaller external applied force  $F_n$ .

In the limit of zero applied force ( $F_n = 0$ ), the JKR model predicts a finite contact radius  $a_0$ :

$$a_0 = \left( \frac{9\pi\gamma R^2}{E^{\dot{c}}} \right)^{\frac{1}{3}} \quad (1.58)$$

It is possible to apply a negative external force to overcome adhesion. The contact radius reduces up to a critical value, after which the contact is broken and the stress is suddenly released (pull-off, PO). The critical pull-off force  $F_{JKR,PO}$  can be obtained from eq. (1.56) by noticing that the term under the square root must be non-negative, i.e.  $12\pi\gamma R F_n + (6\pi\gamma R)^2 \geq 0$ , and finding the force for which the equality strictly holds:

<sup>8</sup> In the following formulas, the same surface energy  $\gamma$  is used for both contacting surfaces, surfaces, so that the work of adhesion  $W$  per unit area required to separate the two surfaces is  $W = -2\gamma$ . This definition may vary for different references. In the general case of different surface energies  $\gamma_1$  and  $\gamma_2$ , the work of adhesion is  $W = -(\gamma_1 + \gamma_2 - \gamma_{12})$ , where  $\gamma_{12}$  is the interfacial energy.

$$F_{JKR,PO} = -3\pi\gamma R \quad (1.59)$$

Interestingly, the pull-off force is independent on the Young's modulus of the material. The pull-off force is typically measured from a force-distance curve recorded with the AFM as the depth of the adhesion well in the retracting branch. In principle, measuring the pull-off force, knowing the radius of the probe, can provide for both the JKR and the DMT models the surface energy  $\gamma$ , through eqs (1.59) and (1.65).

In the JKR model, the contact radius  $a$  does not go smoothly to zero, but at pull-off it is still finite and equal to:

$$a_{PO} = \left( \frac{9\pi\gamma R^2}{4E^i} \right)^{\frac{1}{3}} \quad (1.60)$$

i.e.  $a_{PO} \approx 0.63a_0$ .

The Hertzian formula  $a = \sqrt{R\delta}$  does not hold for the JKR model and the following equation replaces the Hertzian one:

$$\delta = \frac{a^2}{R} - \frac{2}{3} \sqrt{\frac{9\pi\gamma a}{E^i}} \quad (1.61)$$

where the contact radius for a given indentation is larger than for the non-adhesive case because of the surface energy.

In the case of the JKR model, it is not possible to obtain a single equation relating the applied force  $F_n$  and the indentation  $\delta$ , as for the Hertz model. Nevertheless, it is possible to obtain a system of equations, which can be solved recursively to obtain the force-indentation relationship, similarly to the case of the non-adhesive Sneddon model for the spherical indenter eq. (1.13). This system of equations consists of eqs (1.58), (1.60), and (1.62). Alternatively, in this system eq. (1.58) can be replaced by eq. (1.63), obtained from eqs. (1.56), (1.57) after specifying the pull-off force  $F_{JKR,PO}$  using eq.(1.60). eq. (1.63) has the advantage that it depends on the measurable forces  $F_n$  and  $F_{JKR,PO}$ , and the contact radius  $a$  appears only in the right side:

$$\left( \sqrt{F_n + |F_{JKR,PO}|} + \sqrt{|F_{JKR,PO}|} \right)^2 = \frac{4}{3} \frac{E^i}{R} a^3 \quad (1.62)$$

The DMT model is derived from the Derjaguin approximation (Derjaguin, 1934), and assumes that the adhesion only acts outside the contact area, which is negligibly small; this assumption leads to a constant adhesive force  $F_{adh} = 4\pi\gamma R$  (see footnote <sup>9</sup>), which adds to the external applied force  $F_n$ , determining a total normal force, which causes an increased radius of contact  $a$ , as in the case of the JKR model. At odd with the JKR case, however, the adhesion force does not increase with indentation and does not depend on the elastic properties of the sample.

<sup>9</sup> According to the Derjaguin approximation, the force between a curved surface of radius  $R$  and a flat surface is equal to  $F = 2\pi RW$ , where  $W$  is the interaction energy per unit area. Assuming  $W = 2\gamma$  and neglecting the area of the contact, this leads to a constant adhesion force  $F_{adh} = 4\pi\gamma R$ .

Thus, force versus contact radius relationship is still Hertzian, but with a total normal force  $F_n + 4\pi\gamma R$ .

$$F_n + 4\pi\gamma R = \frac{4}{3} \frac{E^i}{R} a^3 \quad (1.63)$$

It follows that a force-indentation relationship similar to the Hertz model holds, with a constant force offset:

$$F_n = \frac{4}{3} E^i \sqrt{R} \delta^{\frac{3}{2}} - 4\pi\gamma R \quad (1.64)$$

Here, the critical or pull-off negative force, at which the tip detaches from the sample, is

$$F_{DMT,PO} = -4\pi\gamma R \quad (1.65)$$

and the radius of contact at pull-off is zero, at odd with the JKR case.

The JKR and DMT models are not commonly used for cell and tissue measurements, where it is typically assumed that non-specific adhesion is negligible but may help in realising on the effect of adhesion on the measured elastic parameters. This is particularly true for the DMT model, where only adhesion forces outside the contact region, *i.e.* over a distance are considered. Usually this could be due to van der Waals forces which act over 100s of nm and will always be attractive (except some exotic special cases). Since in cells, long range van der Waals forces are compensated by long range polymer forces (generated by the glycocalix) of cells, we expect that this model is not relevant for interactions between cells and probes. The JKR model, on the other side assumes wetting like adhesion between the sample and the probe, characterized by a surface energy  $\gamma$ . A wetting like behaviour has been described for spreading and adhesion of cells on solid supports by Sackmann and Bruinsma (Sackmann and Bruinsma, 2002). However, this process is slow, since it requires diffusion of adhesion molecules on the cell surface, which requires some time to establish. Thus, it is safe, for most applications, where contact time is short (below 1 second) that adhesion forces can be neglected in AFM mechanical data. The force-indentation functions of the JKR and DMT models considering adhesion are listed below in table Table 4:

**Table 4** Force-indentation function of the JKR and DMT models considering adhesion, where  $F_n$  is the applied normal force and  $F_{PO}$  is the pull-off force.

Probe geometry	Force-indentation function, $F(\delta)$	Reference	Limits of validity
<b>JKR Model</b>  <b>Sphere of radius R</b>	$\left\{ \begin{aligned} \left( \sqrt{F_n +  F_{JKR,PO} } + \sqrt{ F_{JKR,PO} } \right)^2 &= \frac{4}{3} \frac{E^i}{R} a^3 \\ \delta &= \frac{a^2}{R} - \frac{2}{3} \sqrt{\frac{9\pi\gamma a}{E^i}} \\ F_{JKR,PO} &= -3\pi\gamma R \end{aligned} \right.$	(Johnson et al., 1971) Other probe shapes (Popov et al., 2019b)	short-range adhesive interactions deformable interface/large probe (large contact area)

<b>DMT Model</b>  <b>Sphere of radius R</b>	$F_n = \frac{4}{3} E^* \sqrt{R} \delta^{\frac{3}{2}} -  F_{DMT,PO} $ $F_{DMT,PO} = -4 \pi \gamma R$	(Derjaguin et al., 1975)	long-ranged adhesive interactions rigid interface/small probe (small contact area)
---	---	--------------------------	--

### Thin shells

The theoretical framework described so far to determine the mechanical properties of living cells assumes a contact between two solid bodies. This has been shown to be a good description for eukaryotic cells, but might not be the case for other types of cells, such as bacteria or plant cells. In that case, unlike the very compliant plasma membrane of eukaryotic cells, bacteria present a rigid cell wall that may be deformed by bending at very small depths caused by the AFM tip. Thus, the theory described above may not be valid except for a very small indentation depth (Loskill et al., 2014). In case for larger deformations, the theory of thin shells has been used. The simplest model might be that of a convex spherical cap of thickness  $h$  and radius  $R$  loaded by a force  $F$  (the AFM tip) at one point. In this context, we can define two characteristic quantities, the bending stiffness:

$$K = \frac{Eh^3}{12(1-\nu^2)} \quad (1.66)$$

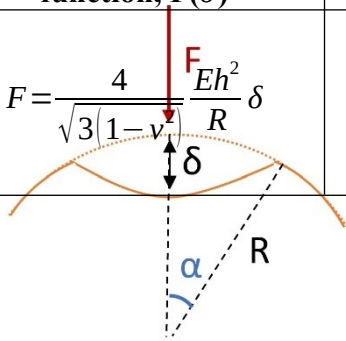
and the extensional stiffness:

$$\eta = \frac{Eh}{(1-\nu^2)} \quad (1.67)$$

The relationship between force and deformation can be derived assuming that bending prevails over stretching and that the deformation  $\delta$  and thickness  $h$  of the shell are much smaller than the radius of the spherical cap ( $\delta, h \ll R$ ), as shown in figure Figure 1-7 Schematic drawing of the Landau and Lifshitz thin film model (Landau and Lifshitz, 1986)., (Landau and Lifshitz, 1986)

$$F = \frac{4}{\sqrt{3(1-\nu^2)}} \frac{Eh^2}{R} \delta. \quad (1.68)$$

As can be seen from the equation above, the force-deformation relationship is linear in this

Probe geometry	Force-indentation function, $F(\delta)$	Reference	Limits of validity
Thin spherical shell stiffer than the material inside with thickness $h$ and radius $R$	$F = \frac{4}{\sqrt{3(1-\nu)}} \frac{F E h^2}{R} \delta$ 	(Landau and Lifshitz, 1986)	$\delta, h \ll R$

**Figure 1-7** Schematic drawing of the Landau and Lifshitz thin film model (Landau and Lifshitz, 1986).

case, with a slope being related to the geometry ( $R, h$ ) and the mechanical properties of the shell ( $E, \nu$ ). This theoretical framework has been used, for example, to determine the stiffness of microcapsules or bacterial cell walls (Arnoldi et al., 2000; Dubreuil et al., 2003; Fery and Weinkamer, 2007; Gaboriaud et al., 2005). The force-indentation equation corresponding to the thin shell model is shown in tTable 5.

**Table 5** Thin shell model

## 1.7 Finite element modelling

In the previous sections of this chapter, we presented some of the principal analytical solutions of contact problems for configurations commonly used in indenter experiments. As we explained, these analytical solutions can be obtained when the symmetry of the contact between the two bodies allows to simplify the geometry of the contact problem. This is possible when the external force applied is normal to the sample's surface and when the probe geometry is axisymmetric, the bodies are isotropic and the strains are small (even if some analytical solutions are available also for tangent contact (Popov et al., 2019a). These important assumptions allow the method of dimensionality reduction (MDR) (Popov and Heß, 2013, 2015)) to reduce a three-dimensional contact mechanics problem to a two-dimensional problem.

This reduction, thus, is not always possible with all the probe geometries and the analytical solutions described in the previous sections are accurate only within the limits of validity mentioned for each model. In the cases in which analytical solutions are difficult to achieve, because of the complexity of the contact problem resulting from intricate geometries of contacting bodies, or from large deformations and nonlinear materials, the most general Bousinesq problem of stresses and deformations or strains arising from to bodies in contact can often be solved numerically. In these cases, the stress-strain relation cannot be anymore simplified and in the case of a linear elastic material, it is described by the following general equation:

$$\sigma = D : \varepsilon, \sigma_{ij} = D_{ijkl} \varepsilon_{kl} \quad (1.1.69)$$

Where  $\sigma$  is the rank-2 stress tensor,  $\varepsilon$  the rank-2 strain tensor and  $D$  is a rank-4 elasticity tensor. At this point many contact mechanics problems are described by the theory of mechanics of continuum bodies, where the structural problem is formulated as a set of differential equations that are satisfied at every point in the domain. The system of differential

equations is obtained considering the principal three fundamental laws of mechanics: conservation of mass, conservation of linear momentum, and conservation of angular momentum.

The principle of the conservation of mass allows a Lagrangian description of the contact problem, the principle of the conservation of the angular momentum guarantees that the stress tensor is symmetric, while the principle of conservation of linear momentum is imposed on an infinitesimal element of a structure to impose the principle of force equilibrium and obtain a system of partial differential equations (PDE) along with boundary conditions, that is called the boundary-valued problem (BVP). If the system is conservative, also a variational method based on the principle of minimum potential energy can be developed to solve the problem.

The principal numerical implementations to solve variational equations or BVP problems, widely used and validated are the finite element method (FEM) and boundary element method (BEM). While the BEM have been used for general contact problems, the FEM method is specific for solid mechanics. An exhaustive description of the numerical methods, with the derivation of all the equations, would need a specific manual, which goes beyond the aim of this chapter. Accordingly, we just briefly illustrate the basic concept of the FEM method, specific for solid mechanics, and we refer to more exhaustive works for further details.

The FEM method allows to solve partial differential equations in two or three space variables. FEM analysis is widely used in many fields of physics or mechanical engineering to solve linear or non-linear problems, which cannot be solved analytically, such as contact problems for the study of the mechanical properties of new materials, climate models for atmospherical predictions, mechanical problems related to seismology and geophysics and many others. Nowadays, the FEM method is very used in several fields of industry, such as: biomechanical industry for the design of new prothesis, cosmetics, aeronautical or automotive industry to study the resistance of new materials to heat and impact, for example in case of vehicle crash. The method consists in simplifying a complex problem, dividing a large system in smaller subunits (Example of a finite element simulation for a rigid indenter indenting orthogonally a soft semi-infinite half space in the case of large deformations, using finite element package ANSYS . The figure is reproduced from Wu et al. () with the permission of Elsevier., for which the solution is simpler. The small subunits are called finite elements.

The subunits are obtained thanks to a discretization of the space in two or three dimensions,

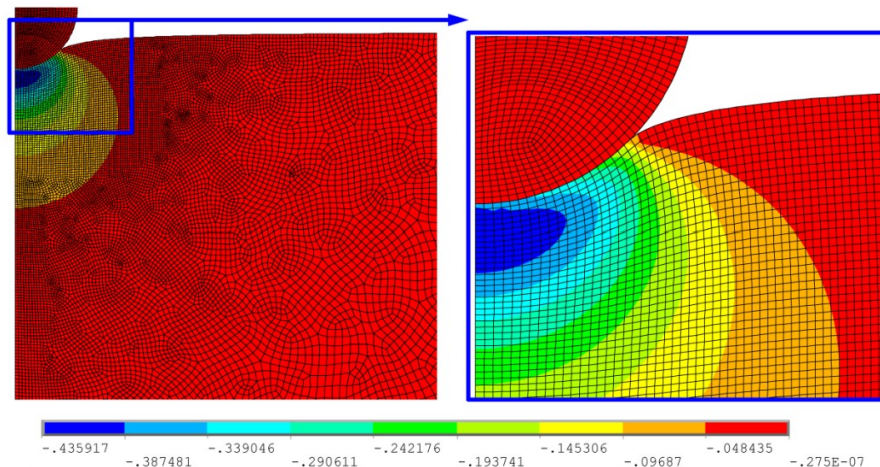


**Figure 1-8** Example of a finite element simulation for a rigid indenter indenting orthogonally a soft semi-infinite half space in the case of large deformations, using finite element package ANSYS . The figure is reproduced from Wu et al. () with the permission of Elsevier.

implementing a mesh of the object with finite number of points, that is the domain of the unknown function. Indeed, per each finite element, simpler equations are defined, which are



(Wu et al., 2016) then assembled in a large system of algebraic equations over the entire domain.

The finite elements are connected through nodes to the adjacent elements. The variational equation solution of each finite element is then not solved analytically, but it is approximated in a polynomial form for the solution of the entire problem. The approximate solution  $u(x)$  is expressed as a sum of a number of functions that are called trial functions, as shown in figure Figure 1-9. The FEM analysis applied in contact mechanics can answer the following

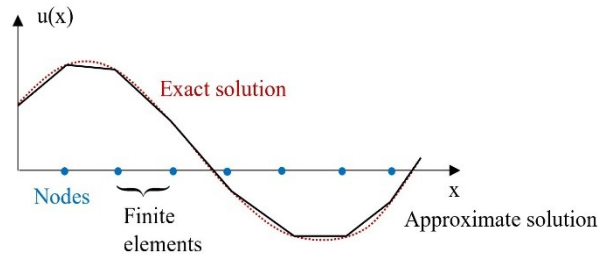


**Figure 1-9** Graphical representation of the linear approximation for the function  $u(x)$  with the finite element method used to solve a one-dimensional problem, as described by Kim (Kim 2015).

questions: 1) if two or more bodies are in contact, 2) where is and what is the region of contact, 3) how much force and pressure is distributed in the contact interface, 4) the magnitude and distribution of the strains in the material due to the stresses and 5) the relative motion in general of the bodies after the contact. Therefore, the FEM method can be very useful to study contact problems that are not solvable analytically, but can be used also as supportive study to validate a contact mechanics analytical model. Indeed, FEM analysis can provide some additional information, for example the lateral displacements due to the probe indentation of a soft material, which are not considered in analytical models due to the assumption of perfect normal penetration of the indenter.

In many recent works, in which contact mechanics models are developed, the results of the analytical model are compared to those ones obtained thanks to a FEM analysis, in order to validate the analytical model. For example, in Efremov et al., Doss et al. and in Garcia et al. (Doss et al., 2019; Efremov et al., 2020; Garcia, 2020) the FEM simulations were used to compare different models (or just numerical, or numerical and analytical) to then choose the theoretical approach that could better model the experimental data.

The principal steps for the contact analysis with FEM method are:

1. Defining the problem geometry and the contact pairs and types
2. searching for the contact point
3. calculating contact force and tangent stiffness

The detailed explanation of these three steps and the relative equations are described in a comprehensive but didactic manner in the book *Introduction to Nonlinear Finite Element Analysis* by Nam-Ho Kim (Kim, 2015), where a section is also dedicated to the Matlab implementation of FEM analysis for contact mechanics problems and where some Matlab codes are available. Apart from Matlab FEM implementation, several software tools are nowadays available for a user-friendly application of FEM analysis, some are for example: ANSYS, COMSOL software (COMSOL Multiphysics; COMSOL AB, Stockholm, Sweden) and Abaqus CAE (Simulia Corp. Providence, RI).

## 1.8 Concluding remarks

In this chapter, we have tried to provide the most used contact models to describe AFM measurements on cells and tissues. Those included purely elastic bodies, viscoelastic, finite bodies and adhesion. There are, of course, a large number of models that were not considered. For example, models including different layers of materials with varying elasticity, models considering surface tension and nonlinear materials (Bhushan and Peng, 2002). We have also constrained to models used to fit the force-indentation curves. Other approaches such as the Oliver and Pharr method, widely used in material science, or the early A-Hassan approach, developed for AFM measurements on cells, have been omitted as they can be derived from the formalism used here (A-Hassan et al., 1998; Lin et al., 2008; Pharr et al., 1992). Given the widespread of AFM as a nanomechanical tool in biology and given the heterogeneity and nonlinearity of biological samples, we expect the emergence of more sophisticated approaches and derivations likely involving computer simulations that would move further and further away from the seminal Hertz model.

## 1.9 Acknowledgements

The authors thank Andreas Janshoff and Javier López for insightful discussions. We acknowledge the support of the European Union's Horizon 2020 research and innovation programme under the Marie Skłodowska-Curie grant agreement No 713750, Project DOC2AMU. Also, it has been carried out with the financial support of the Regional Council of Provence- Alpes-Côte d'Azur and with the financial support of the A\*MIDEX (n° ANR-11-IDEX-0001-02), funded by the Investissements d'Avenir project funded by the French Government, managed by the French National Research Agency (ANR). This project has received funding from the European Research Council (ERC, grant agreement No 772257) and from the Human Frontier Science Program (HFSP, grant No. RGP0056/2018). The authors thank Elsevier for the permission of the free reuse of figure 3 in Wu et al for figure 8.

## Bibliography

A-Hassan, E., Heinz, W., Antonik, M., D'Costa, N., Nageswaran, S., Schoenenberger, C.-A., and Hoh, J. (1998). Relative Microelastic Mapping of Living Cells by Atomic Force Microscopy. *Biophysical Journal* 74, 1564–1578. [https://doi.org/10.1016/S0006-3495\(98\)77868-3](https://doi.org/10.1016/S0006-3495(98)77868-3).

Akhremitchev, B.B., and Walker, G.C. (1999). Finite Sample Thickness Effects on Elasticity Determination Using Atomic Force Microscopy. *Langmuir* 15, 5630–5634. <https://doi.org/10.1021/la980585z>.

Alcaraz, J., Buscemi, L., Grabulosa, M., Trepate, X., Fabry, B., Farré, R., and Navajas, D. (2003). Microrheology of Human Lung Epithelial Cells Measured by Atomic Force Microscopy. *Biophysical Journal* 84, 2071–2079. [https://doi.org/10.1016/S0006-3495\(03\)75014-0](https://doi.org/10.1016/S0006-3495(03)75014-0).

Aleksandrov, V.M. (1968). Asymptotic methods in contact problems of elasticity theory: *PMM* vol.32, N<sup>o</sup>4, 1968, pp.672–683. *Journal of Applied Mathematics and Mechanics* 32, 691–703. [https://doi.org/10.1016/0021-8928\(68\)90099-3](https://doi.org/10.1016/0021-8928(68)90099-3).

Aleksandrov, V.M. (1969). Asymptotic solution of the contact problem for a thin elastic layer: *PMM* vol. 33, no. 1, 1969, pp. 61–73. *Journal of Applied Mathematics and Mechanics* 33, 49–63. [https://doi.org/10.1016/0021-8928\(69\)90113-0](https://doi.org/10.1016/0021-8928(69)90113-0).

- Arnoldi, M., Fritz, M., Bäuerlein, E., Radmacher, M., Sackmann, E., and Boulbitch, A. (2000). Bacterial turgor pressure can be measured by atomic force microscopy. *Phys. Rev. E* 62, 1034–1044. <https://doi.org/10.1103/PhysRevE.62.1034>.
- Balland, M., Desprat, N., Icard, D., Féréol, S., Asnacios, A., Browaeys, J., Hénon, S., and Gallet, F. (2006). Power laws in microrheology experiments on living cells: Comparative analysis and modeling. *Phys. Rev. E* 74, 021911. <https://doi.org/10.1103/PhysRevE.74.021911>.
- Barber, J.R., and Billings, D.A. (1990). An approximate solution for the contact area and elastic compliance of a smooth punch of arbitrary shape. *International Journal of Mechanical Sciences* 32, 991–997. [https://doi.org/10.1016/0020-7403\(90\)90003-2](https://doi.org/10.1016/0020-7403(90)90003-2).
- Betti, E. (1872). Teoria dell'elasticità. *Il Nuovo Cimento Serie 2. Volume VII-VIII*, 69–97. .
- Bhushan, B., and Peng, W. (2002). Contact mechanics of multilayered rough surfaces. *Appl. Mech. Rev* 55, 435–480. <https://doi.org/10.1115/1.1488931>.
- Bilodeau, G.G. (1992). Regular Pyramid Punch Problem. *Journal of Applied Mechanics* 59, 519–523. <https://doi.org/10.1115/1.2893754>.
- Boussinesq, J. (1885). Application des potentiels à l'étude de l'équilibre et du mouvement des solides élastiques, principalement au calcul des déformations et des pressions que produisent, dans ces solides, des efforts quelconques exercés sur une petite partie de leur surface ou de leur intérieur : mémoire suivi de notes étendues sur divers points de physique mathématique et d'analyse. Lilliad - Université de Lille - Sciences et technologies.
- Briscoe, B.J., Sebastian, K.S., and Adams, M.J. (1994). The effect of indenter geometry on the elastic response to indentation. *J. Phys. D: Appl. Phys.* 27, 1156–1162. <https://doi.org/10.1088/0022-3727/27/6/013>.
- Brückner, B.R., Nöding, H., and Janshoff, A. (2017). Viscoelastic Properties of Confluent MDCK II Cells Obtained from Force Cycle Experiments. *Biophysical Journal* 112, 724–735. <https://doi.org/10.1016/j.bpj.2016.12.032>.
- Chadwick, R.S. (2002). Axisymmetric Indentation of a Thin Incompressible Elastic Layer. *SIAM J. Appl. Math.* 62, 1520–1530. <https://doi.org/10.1137/S0036139901388222>.
- Chen, W.T., and Engel, P.A. (1972). Impact and contact stress analysis in multilayer media. *International Journal of Solids and Structures* 8, 1257–1281. [https://doi.org/10.1016/0020-7683\(72\)90079-0](https://doi.org/10.1016/0020-7683(72)90079-0).
- Chyasnavichyus, M., Young, S.L., Geryak, R., and Tsukruk, V.V. (2016). Probing elastic properties of soft materials with AFM: Data analysis for different tip geometries. *Polymer* 102, 317–325. <https://doi.org/10.1016/j.polymer.2016.02.020>.
- Darling, E.M., Zauscher, S., Block, J.A., and Guilak, F. (2007). A Thin-Layer Model for Viscoelastic, Stress-Relaxation Testing of Cells Using Atomic Force Microscopy: Do Cell Properties Reflect Metastatic Potential? *Biophysical Journal* 92, 1784–1791. <https://doi.org/10.1529/biophysj.106.083097>.
- Derjaguin, B. (1934). Untersuchungen über die Reibung und Adhäsion, IV. *Kolloid-Zeitschrift* 69, 155–164. <https://doi.org/10.1007/BF01433225>.

Derjaguin, B.V., Muller, V.M., and Toporov, Yu.P. (1975). Effect of contact deformations on the adhesion of particles. *Journal of Colloid and Interface Science* 53, 314–326. [https://doi.org/10.1016/0021-9797\(75\)90018-1](https://doi.org/10.1016/0021-9797(75)90018-1).

D. Garcia, P., R. Guerrero, C., and Garcia, R. (2020). Nanorheology of living cells measured by AFM-based force–distance curves. *Nanoscale* 12, 9133–9143. <https://doi.org/10.1039/C9NR10316C>.

Dhaliwal, R.S., and Rau, I.S. (1970). The axisymmetric boussinesq problem for a thick elastic layer under a punch of arbitrary profile. *International Journal of Engineering Science* 8, 843–856. [https://doi.org/10.1016/0020-7225\(70\)90086-8](https://doi.org/10.1016/0020-7225(70)90086-8).

Dimitriadis, E.K., Horkay, F., Maresca, J., Kachar, B., and Chadwick, R.S. (2002). Determination of Elastic Moduli of Thin Layers of Soft Material Using the Atomic Force Microscope. *Biophysical Journal* 82, 2798–2810. [https://doi.org/10.1016/S0006-3495\(02\)75620-8](https://doi.org/10.1016/S0006-3495(02)75620-8).

Doss, B.L., Eliato, K.R., Lin, K., and Ros, R. (2019). Quantitative mechanical analysis of indentations on layered, soft elastic materials. *Soft Matter* 15, 1776–1784. <https://doi.org/10.1039/C8SM02121J>.

Dubreuil, F., Elsner, N., and Fery, A. (2003). Elastic properties of polyelectrolyte capsules studied by atomic-force microscopy and RICM. *Eur. Phys. J. E* 12, 215–221. <https://doi.org/10.1140/epje/i2003-10056-0>.

Efremov, Y.M., Wang, W.-H., Hardy, S.D., Geahlen, R.L., and Raman, A. (2017). Measuring nanoscale viscoelastic parameters of cells directly from AFM force-displacement curves. *Sci Rep* 7, 1541. <https://doi.org/10.1038/s41598-017-01784-3>.

Efremov, Y.M., Kotova, S.L., and Timashev, P.S. (2020). Viscoelasticity in simple indentation-cycle experiments: a computational study. *Sci Rep* 10, 13302. <https://doi.org/10.1038/s41598-020-70361-y>.

Fabrikant, V.I. (1986). Flat punch of arbitrary shape on an elastic half-space. *International Journal of Engineering Science* 24, 1731–1740. [https://doi.org/10.1016/0020-7225\(86\)90078-9](https://doi.org/10.1016/0020-7225(86)90078-9).

Fabry, B., Maksym, G.N., Butler, J.P., Glogauer, M., Navajas, D., and Fredberg, J.J. (2001). Scaling the Microrheology of Living Cells. *Phys. Rev. Lett.* 87, 148102. <https://doi.org/10.1103/PhysRevLett.87.148102>.

Fery, A., and Weinkamer, R. (2007). Mechanical properties of micro- and nanocapsules: Single-capsule measurements. *Polymer* 48, 7221–7235. <https://doi.org/10.1016/j.polymer.2007.07.050>.

Gaboriaud, F., Bailet, S., Dague, E., and Jorand, F. (2005). Surface Structure and Nanomechanical Properties of *Shewanella putrefaciens* Bacteria at Two pH values (4 and 10) Determined by Atomic Force Microscopy. *Journal of Bacteriology* 187, 3864–3868. <https://doi.org/10.1128/JB.187.11.3864-3868.2005>.

Garcia, R. (2020). Nanomechanical mapping of soft materials with the atomic force microscope: methods, theory and applications. *Chemical Society Reviews* 49, 5850–5884. <https://doi.org/10.1039/D0CS00318B>.

- Garcia, P.D., and Garcia, R. (2018a). Determination of the Elastic Moduli of a Single Cell Cultured on a Rigid Support by Force Microscopy. *Biophysical Journal* *114*, 2923–2932. <https://doi.org/10.1016/j.bpj.2018.05.012>.
- Garcia, P.D., and Garcia, R. (2018b). Determination of the viscoelastic properties of a single cell cultured on a rigid support by force microscopy. *Nanoscale* *10*, 19799–19809. <https://doi.org/10.1039/C8NR05899G>.
- Gavara, N. (2016). Combined strategies for optimal detection of the contact point in AFM force-indentation curves obtained on thin samples and adherent cells. *Sci Rep* *6*, 21267. <https://doi.org/10.1038/srep21267>.
- Gavara, N., and Chadwick, R.S. (2012). Determination of the elastic moduli of thin samples and adherent cells using conical atomic force microscope tips. *Nature Nanotechnology*.
- Graham, G.A.C. (1965). The contact problem in the linear theory of viscoelasticity. *International Journal of Engineering Science* *3*, 27–46. [https://doi.org/10.1016/0020-7225\(65\)90018-2](https://doi.org/10.1016/0020-7225(65)90018-2).
- Greenwood, J.A., Williamson, J.B.P., and Bowden, F.P. (1966). Contact of nominally flat surfaces. *Proceedings of the Royal Society of London. Series A. Mathematical and Physical Sciences* *295*, 300–319. <https://doi.org/10.1098/rspa.1966.0242>.
- Hertz, H. (1881). On the contact of elastic bodies. In *Hertz's Miscellaneous Papers* (London: Macmillan, New York, Macmillan and co.).
- Hertz, H. (1882). Ueber die Berührung fester elastischer Körper. *1882*, 156–171. <https://doi.org/10.1515/crll.1882.92.156>.
- Heuberger, M., Dietler, G., and Schlapbach, L. (1996). Elastic deformations of tip and sample during atomic force microscope measurements. *Journal of Vacuum Science & Technology B: Microelectronics and Nanometer Structures Processing, Measurement, and Phenomena* *14*, 1250–1254. <https://doi.org/10.1116/1.588525>.
- Johnson, K.L. (1985). *Contact Mechanics* (Cambridge: Cambridge University Press).
- Johnson, K.L., Kendall, K., Roberts, A.D., and Tabor, D. (1971). Surface energy and the contact of elastic solids. *Proceedings of the Royal Society of London. A. Mathematical and Physical Sciences* *324*, 301–313. <https://doi.org/10.1098/rspa.1971.0141>.
- Jorba, I., Uriarte, J.J., Campillo, N., Farré, R., and Navajas, D. (2017). Probing Micromechanical Properties of the Extracellular Matrix of Soft Tissues by Atomic Force Microscopy. *Journal of Cellular Physiology* *232*, 19–26. <https://doi.org/10.1002/jcp.25420>.
- Kalcioglu, Z.I., Mahmoodian, R., Hu, Y., Suo, Z., and Van Vliet, K.J. (2012). From macro-to microscale poroelastic characterization of polymeric hydrogels via indentation. *Soft Matter* *8*, 3393–3398. .
- Kim, N.-H. (2015). Finite Element Analysis for Contact Problems. In *Introduction to Nonlinear Finite Element Analysis*, N.-H. Kim, ed. (New York, NY: Springer US), pp. 367–426.

Kontomaris, S.V., and Malamou, A. (2021a). A novel approximate method to calculate the force applied on an elastic half space by a rigid sphere. *Eur. J. Phys.* *42*, 025010. <https://doi.org/10.1088/1361-6404/abccfb>.

Kontomaris, S.-V., and Malamou, A. (2021b). Grouping transient phenomena in various physical procedures using elementary mathematical analysis. *Phys. Educ.* *56*, 065027. <https://doi.org/10.1088/1361-6552/ac22bc>.

Landau, L.D., and Lifshitz, E.M. (1986). *Theory of Elasticity - 3rd Edition* (Oxford: Pergamon Press).

Lee, E.H., and Radok, J.R.M. (1960). The Contact Problem for Viscoelastic Bodies. *Journal of Applied Mechanics* *27*, 438–444. <https://doi.org/10.1115/1.3644020>.

Lin, D.C., Dimitriadis, E.K., and Horkay, F. (2008). Robust strategies for automated AFM force curve analysis--I. Non-adhesive indentation of soft, inhomogeneous materials. *J Biomech Eng* *129*, 430–440. <https://doi.org/10.1115/1.2720924>.

Long, R., Hall, M.S., Wu, M., and Hui, C.-Y. (2011). Effects of Gel Thickness on Microscopic Indentation Measurements of Gel Modulus. *Biophys J* *101*, 643–650. <https://doi.org/10.1016/j.bpj.2011.06.049>.

Loskill, P., Pereira, P.M., Jung, P., Bischoff, M., Herrmann, M., Pinho, M.G., and Jacobs, K. (2014). Reduction of the Peptidoglycan Crosslinking Causes a Decrease in Stiffness of the *Staphylococcus aureus* Cell Envelope. *Biophysical Journal* *107*, 1082–1089. <https://doi.org/10.1016/j.bpj.2014.07.029>.

Love, A.E.H. (1929). IX. The stress produced in a semi-infinite solid by pressure on part of the boundary. *Philosophical Transactions of the Royal Society of London. Series A, Containing Papers of a Mathematical or Physical Character* *228*, 377–420. <https://doi.org/10.1098/rsta.1929.0009>.

Love, A.E.H. (1939). Boussinesq's problem for a rigid cone. *The Quarterly Journal of Mathematics os-10*, 161–175. <https://doi.org/10.1093/qmath/os-10.1.161>.

Mahaffy, R.E., Shih, C.K., MacKintosh, F.C., and Käs, J. (2000). Scanning Probe-Based Frequency-Dependent Microrheology of Polymer Gels and Biological Cells. *Phys. Rev. Lett.* *85*, 880–883. <https://doi.org/10.1103/PhysRevLett.85.880>.

Managuli, V., and Roy, S. (2018). Asymptotical Correction to Bottom Substrate Effect Arising in AFM Indentation of Thin Samples and Adherent Cells Using Conical Tips. *Exp Mech* *58*, 733–741. <https://doi.org/10.1007/s11340-018-0373-8>.

Maugis, D. (1992). Adhesion of spheres: The JKR-DMT transition using a dugdale model. *Journal of Colloid and Interface Science* *150*, 243–269. [https://doi.org/10.1016/0021-9797\(92\)90285-T](https://doi.org/10.1016/0021-9797(92)90285-T).

Moeendarbary, E., Valon, L., Fritzsche, M., Harris, A.R., Moulding, D.A., Thrasher, A.J., Stride, E., Mahadevan, L., and Charras, G.T. (2013). The cytoplasm of living cells behaves as a poroelastic material. *Nature Materials* *12*, 253–261. <https://doi.org/10.1038/nmat3517>.

Müller, P., Abuhattum, S., Möllmert, S., Ulbricht, E., Taubenberger, A.V., and Guck, J. (2019). nanite: using machine learning to assess the quality of atomic force microscopy-

enabled nano-indentation data. *BMC Bioinformatics* 20, 465. <https://doi.org/10.1186/s12859-019-3010-3>.

Pharr, G.M., Oliver, W.C., and Brotzen, F.R. (1992). On the generality of the relationship among contact stiffness, contact area, and elastic modulus during indentation. *Journal of Materials Research* 7, 613–617. <https://doi.org/10.1557/JMR.1992.0613>.

Popov, V.L., and Heß, M. (2013). *Methode der Dimensionsreduktion in Kontaktmechanik und Reibung* (Springer).

Popov, V.L., and Heß, M. (2015). *Method of Dimensionality Reduction in Contact Mechanics and Friction*.

Popov, V.L., Heß, M., and Willert, E. (2019a). *Introduction* (Berlin, Heidelberg: Springer Berlin Heidelberg).

Popov, V.L., Heß, M., and Willert, E. (2019b). Tangential Contact. In *Handbook of Contact Mechanics: Exact Solutions of Axisymmetric Contact Problems*, V.L. Popov, M. Heß, and E. Willert, eds. (Berlin, Heidelberg: Springer), pp. 125–173.

Radmacher, M., Tillmann, R.W., Fritz, M., and Gaub, H.E. (1992). From Molecules to Cells: Imaging Soft Samples with the Atomic Force Microscope. *Science* 257, 1900–1905. <https://doi.org/10.1126/science.1411505>.

Radmacher, M., Fritz, M., Kacher, C.M., Cleveland, J.P., and Hansma, P.K. (1996). Measuring the viscoelastic properties of human platelets with the atomic force microscope. *Biophys J* 70, 556–567. .

Rayleigh, Lord (1873). Note on the Numerical Calculation of the Roots of Fluctuating Functions. *Proceedings of the London Mathematical Society s1-5*, 119–124. <https://doi.org/10.1112/plms/s1-5.1.119>.

Rheinlaender, J., Dimitracopoulos, A., Wallmeyer, B., Kronenberg, N.M., Chalut, K.J., Gather, M.C., Betz, T., Charras, G., and Franze, K. (2020). Cortical cell stiffness is independent of substrate mechanics. *Nat. Mater.* 19, 1019–1025. <https://doi.org/10.1038/s41563-020-0684-x>.

Rico, F., Roca-Cusachs, P., Gavara, N., Farré, R., Rotger, M., and Navajas, D. (2005). Probing mechanical properties of living cells by atomic force microscopy with blunted pyramidal cantilever tips. *Phys. Rev. E* 72, 021914. <https://doi.org/10.1103/PhysRevE.72.021914>.

Rico, F., Roca-Cusachs, P., Sunyer, R., Farré, R., and Navajas, D. (2007). Cell dynamic adhesion and elastic properties probed with cylindrical atomic force microscopy cantilever tips. *J Mol Recognit* 20, 459–466. <https://doi.org/10.1002/jmr.829>.

Rigato, A., Miyagi, A., Scheuring, S., and Rico, F. (2017). High-frequency microrheology reveals cytoskeleton dynamics in living cells. *Nature Phys* 13, 771–775. <https://doi.org/10.1038/nphys4104>.

Sackmann, E., and Bruinsma, R. (2002). Cell Adhesion as Wetting Transition? In *Physics of Bio-Molecules and Cells. Physique Des Biomolécules et Des Cellules*, F. Flyvbjerg, F. Jülicher, P. Ormos, and F. David, eds. (Berlin, Heidelberg: Springer), pp. 285–309.

Shield, R.T. (1967). Load-displacement relations for elastic bodies. *Journal of Applied Mathematics and Physics (ZAMP)* 18, 682–693. <https://doi.org/10.1007/BF01602041>.

Slaughter, W.S. (2002). Linearized Elasticity Problems. In *The Linearized Theory of Elasticity*, W.S. Slaughter, ed. (Boston, MA: Birkhäuser), pp. 221–254.

Sneddon, I.N. (1965). The relation between load and penetration in the axisymmetric boussinesq problem for a punch of arbitrary profile. *International Journal of Engineering Science* 3, 47–57. [https://doi.org/10.1016/0020-7225\(65\)90019-4](https://doi.org/10.1016/0020-7225(65)90019-4).

Tabor, D. (1977). Surface forces and surface interactions. *Journal of Colloid and Interface Science* 58, 2–13. [https://doi.org/10.1016/0021-9797\(77\)90366-6](https://doi.org/10.1016/0021-9797(77)90366-6).

Ting, T.C.T. (1966). The Contact Stresses Between a Rigid Indenter and a Viscoelastic Half-Space. *Journal of Applied Mechanics* 33, 845–854. <https://doi.org/10.1115/1.3625192>.

Tu, Y.-O., and Gazis, D.C. (1964). The Contact Problem of a Plate Pressed Between Two Spheres. *Journal of Applied Mechanics* 31, 659–666. <https://doi.org/10.1115/1.3629728>.

Wu, C.-E., Lin, K.-H., and Juang, J.-Y. (2016). Hertzian load–displacement relation holds for spherical indentation on soft elastic solids undergoing large deformations. *Tribology International* 97, 71–76. <https://doi.org/10.1016/j.triboint.2015.12.034>.

Yang, F. (1998). Indentation of an incompressible elastic film. This work was finished when the author was at the University of Rochester, Rochester, NY, USA. *Mechanics of Materials* 30, 275–286. [https://doi.org/10.1016/S0167-6636\(98\)00035-0](https://doi.org/10.1016/S0167-6636(98)00035-0).